Submitted to Nuclear Physics B

UCRL-20269
Preprint

RECEIVED
LAWRENCE
RADIATION LABORATORY

DOCUMENTS SECTION

A STUDY OF K^+d INTERACTIONS FROM 865 TO 1585 MeV/c

A. A. Hirata, G. Goldhaber, V. H. Seeger,
G. H. Trilling, and C. G. Wohl

May 18, 1971

AEC Contract No. W-7405-eng-48

TWO-WEEK LOAN COPY

This is a Library Circulating Copy which may be borrowed for two weeks. For a personal retention copy, call Tech. Info. Division, Ext. 5545

UCRL-20269

LAWRENCE RADIATION LABORATORY
UNIVERSITY of CALIFORNIA BERKELEY

DISCLAIMER

This document was prepared as an account of work sponsored by the United States Government. While this document is believed to contain correct information, neither the United States Government nor any agency thereof, nor the Regents of the University of California, nor any of their employees, makes any warranty, express or implied, or assumes any legal responsibility for the accuracy, completeness, or usefulness of any information, apparatus, product, or process disclosed, or represents that its use would not infringe privately owned rights. Reference herein to any specific commercial product, process, or service by its trade name, trademark, manufacturer, or otherwise, does not necessarily constitute or imply its endorsement, recommendation, or favoring by the United States Government or any agency thereof, or the Regents of the University of California. The views and opinions of authors expressed herein do not necessarily state or reflect those of the United States Government or any agency thereof or the Regents of the University of California.

UCRL-20269

A STUDY OF K^+d INTERACTIONS FROM 865 TO 1585 MeV/c*

A. A. Hirata,† G. Goldhaber, V. H. Seeger,‡
G. H. Trilling, and C. G. Wohl††

Department of Physics and Lawrence Radiation Laboratory
University of California, Berkeley, California 94720

May 18, 1971

Abstract: We present experimental results on K^+d interactions from 865 to 1585 MeV/c incident beam momentum. We report measurements of several K^+d partial cross sections and calculate most of the others using relations derived from isospin conservation and data from other experiments. The most striking feature of the cross section data is the abrupt rise of the total single-pion-production cross section near 1000 MeV/c. We extract isospin-0 KN partial cross sections and find a rapid increase of $\sigma_0(KN\pi)$ at the threshold for the quasi-two-body reaction $KN \rightarrow K^*N$. As in the case of the isospin-1 K^+N system, it appears that the structure around 1200 MeV/c in the total cross section for the isospin-0 K^+N system is well reconstructed by the sum of three smoothly varying channel cross sections $\sigma_0(KN)$, $\sigma_0(KN\pi)$, and $\sigma_0(KN\pi\pi)$. We study the reaction $KN \rightarrow K^*N$ near threshold and find that the production and decay angular distributions can be interpreted in terms of t-channel phenomena, specifically a superposition of ω, ρ, and π exchange. As is true of the isospin-1 $K\Delta$ and K^*N final states, the isospin-0 K^*N state has a behavior near threshold which is not very different from its behavior at much higher energy.

---

* Work supported by the U. S. Atomic Energy Commission.

† Present address: Department of Natural Philosophy, University of Glasgow, Glasgow, Scotland.

‡ Present address: Department of Physics, San Francisco State College, San Francisco, California 94132.

†† Present address: Nuclear Physics Laboratory, Oxford University, Oxford, England.

1. INTRODUCTION

The K-nucleon system differs from the πN and $\bar{K}N$ systems in that s-channel resonances are either absent or at any rate play a much less prominent role in the low-energy behavior. High precision counter total cross-section measurements have revealed substantial peaks in both isovector and isoscalar KN channels near 1 GeV/c [1]. However, further attempts to determine the nature of the peak for the $I = 1$ KN system, including phase shift analyses of elastic scattering and polarization measurements, and detailed studies of inelastic final states have indicated that [2,3]: (1) a resonance interpretation, while possible, is not a compelling consequence of the data, unlike the case for the πN and $\bar{K}N$ systems; (2) several partial wave amplitudes seem to be significant in the region of the cross-section peak;and, while the $P_{3/2}$ wave is a candidate for an exotic resonance,its energy variation is not more rapid than that of the other waves; (3) the elastic and inelastic scattering angular distributions and polarizations vary slowly and smoothly with energy, extrapolating readily to their high energy t-channel-exchange-dominated characteristics.

The isoscalar KN system is most directly studied by analyzing K^+n interactions, requiring a deuterium target. The complications associated with the extraction of information about K^+n processes from K^+d interactions make the study of the isoscalar KN system more difficult than that of the isovector system. This paper presents the results of a study of K^+n reactions at five different momenta, namely 865, 970, 1210, 1365, and 1585 MeV/c, which are in the region where the total cross-section measurements indicate significant structure. This study was carried out by means of an exposure of the 25-inch LRL bubble chamber filled with deuterium to a separated K^+ beam at the Bevatron.

The processes principally studied include charge exchange and pion production. Detailed consideration of angular distributions in the charge-exchange

process has been given elsewhere [4]. The main emphasis of this paper will be on the cross sections for various final states and the detailed features of pion production, especially production of $K^*(891)$.

2. EXPERIMENTAL DETAILS

The experiment on which this paper is based is a 100,000-picture exposure of the LRL 25-inch deuterium-filled bubble chamber to a separated K^+ beam at the Bevatron. The momenta studied, 865, 970, 1210, 1365, and 1585 MeV/c, are the same as for a companion K^+p experiment whose results have already been published [3].

The film was scanned twice for events with (a) one or more prongs plus Vee and (b) three or more prongs without Vee. Those events with odd numbers of outgoing charged tracks are either K^+ decays or K^+d interactions in which the proton in the deuteron is a spectator to an interaction on the neutron and has too low a momentum (less than $\sim$ 80 MeV/c) to make a visible track. In the latter case, the absence of a track constitutes a measurement (in the sense that one can place an upper limit on its momentum), and in fitting we have assigned to the unseen proton a momentum of zero with an uncertainty appropriate to a proton too slow to be visible.

The initial measurements for this experiment were made on the Berkeley Flying-Spot Digitizer (FSD). Additional measurements and remeasurements were made with "Franckenstein" film-plane measuring projectors. The measurements from the FSD or Franckenstein were processed through the reconstruction and fitting program SIOUX and the analysis program ARROW. Failing events were remeasured until their number was reduced to an insignificant level (less than 5% for all topologies).

In this manner, we found, after all cuts and before weighting, 4299 events with a K^+ and 6670 events with a K^o in the final state. Cross sections were

normalized to 3102 $K^+ \rightarrow \pi^+\pi^-\pi^+$ decays. In obtaining the cross sections, K^o events were corrected for decay via neutral and long-lived modes, decay outside the fiducial volume, and decay too close (less than 2 mm) to the production vertex. Since the scanning efficiency after two complete scans of the film was better than 98%, no correction was made for scanning biases. Furthermore, since the unresolved events were found to be channel independent and since their number was less than the statistical error in most channels we have made no correction for these events. The final source of bias is contamination from incident π^+ interactions. Events with a Vee in the final state were predominantly $K_1^o \rightarrow \pi^+\pi^-$ decays resulting from interactions of incident K^+ mesons. The $\Lambda^o \rightarrow p\pi^-$ decays resulting from incident π^+ interactions could be clearly separated from the $K_1^o \rightarrow \pi^+\pi^-$ decays. Therefore the only channels seriously affected by pion contamination are those in which a K^+ is produced in the final state. For the four lower momenta careful study of bubble density at the scan table was adequate to insure choice of the proper hypothesis. At 1585 MeV/c, a more involved procedure, based on the use of stringent beam entry criteria was successful in reducing the pion contamination to less than 5% [5].

3. CROSS SECTIONS

3.1. K^+d Cross Sections

The reactions that occur at the energies spanned by this experiment are:

$$
\begin{array}{llll}
K^+d \rightarrow KNN \rightarrow K^+pn & & & \\
\qquad\qquad\quad \rightarrow K^opp & & & * \\
\qquad \rightarrow KNN\pi \rightarrow K^+nn\pi^+ & \left.\right\} & \sigma_c & \\
\qquad\qquad\qquad\quad \rightarrow K^opn\pi^+ & & & * \\
\qquad\qquad\qquad\quad \rightarrow K^+pp\pi^- & & & * \\
\qquad\qquad\qquad\quad \rightarrow K^+pn\pi^o & \left.\right\} & \sigma_o & \\
\qquad\qquad\qquad\quad \rightarrow K^opp\pi^o & & & * \\
\qquad \rightarrow KNN\pi\pi \rightarrow K^onn\pi^+\pi^+ & \left.\right\} & \sigma_{cc} & * \\
\qquad\qquad\qquad\quad \rightarrow K^+pn\pi^+\pi^- & & & * \\
\qquad\qquad\qquad\quad \rightarrow K^opp\pi^+\pi^- & & & * \\
\qquad\qquad\qquad\quad \rightarrow K^+nn\pi^+\pi^o & \left.\right\} & \sigma_{co} & \\
\qquad\qquad\qquad\quad \rightarrow K^opn\pi^+\pi^o & & & * \\
\qquad\qquad\qquad\quad \rightarrow K^+pp\pi^-\pi^o & & & * \\
\qquad\qquad\qquad\quad \rightarrow K^+pn\pi^o\pi^o & \left.\right\} & \sigma_{oo} & \\
\qquad\qquad\qquad\quad \rightarrow K^opp\pi^o\pi^o & & . & *
\end{array}
\qquad (1)
$$

Reactions in which the deuteron is left intact are implicitly included with those with a proton and a neutron in the final state. We have measured the cross sections of those reactions marked with an asterisk in (1).

The numbers of events which fit each channel studied are given in table 1. The corresponding cross sections normalized relative to the τ decays are given in the upper part of table 2 and shown in fig. 1a. The charge exchange ($K^+d \rightarrow K^opp$) cross section falls off smoothly with increasing momentum. The single-pion production cross sections all have roughly the same shape, rising rapidly until about 1200 MeV/c and then leveling off. The double-pion production cross sections (only the sum of the measured cross sections--i.e., six of the eight possible channels--is shown) are extremely small until 1200 MeV/c, after which they begin to rise sharply. The thresholds for single and double pion production on deuterons are 450 and 700 MeV/c, and, on free nucleons, are 510 and 810 MeV/c. Evidently the cross sections remain small until the momentum is well above the appropriate threshold.

Hirata et al. [6] have discussed the use of isospin conservation to derive the total one-pion and two-pion production cross sections for K^+d reactions, $\sigma(KNN\pi)$ and $\sigma(KNN\pi\pi)$, and have given results at the four lower momenta 865, 970, 1210 and 1365 MeV/c. We have made the same analysis at 1585 MeV/c. For completeness, the results for all our momenta are shown in fig. 2 and listed in table 2. The $K^+d \rightarrow KNN$ cross sections are obtained by subtraction of the pion channels from the total cross sections.

Figure 2 also shows the total cross-section data of Cool et al. [1], Bugg et al. [1], and Jenkins et al. [7] and some partial cross-section data from Slater et al. [8] and Butterworth et al. [9]. The most striking feature is the abrupt rise of the single-pion production cross section to 15 mb at 1200 MeV/c. Since this rise is accompanied by a less steep fall of the $K^+d \rightarrow KNN$ cross section, the total cross section actually increases in this same momentum interval by only about 10 mb. The onset of double-pion production, by which time the single-pion production cross section has leveled off, has no marked effect on the shape of the total cross section.

3.2. K^+n Pion Production Cross Sections

In order to study the structure in the isospin-0 KN total cross section, we determine the contribution to that cross section from the pion production channels.

There are seven final states for single-pion production and eleven final states for double-pion production:

$$\begin{aligned} K^+p &\rightarrow K^o\pi^+p \\ &\rightarrow K^+\pi^+n \\ &\rightarrow K^+\pi^op \quad , \end{aligned} \tag{2}$$

$$
\begin{aligned}
K^+n &\rightarrow K^o\pi^+n \\
&\rightarrow K^o\pi^op \\
&\rightarrow K^+\pi^-p \\
&\rightarrow K^+\pi^on \quad ,
\end{aligned}
\tag{3}
$$

$$
\begin{aligned}
K^+p &\rightarrow K^on\pi^+\pi^+ \\
&\rightarrow K^+p\pi^+\pi^- \\
&\rightarrow K^+n\pi^+\pi^o \\
&\rightarrow K^op\pi^+\pi^o \\
&\rightarrow K^+p\pi^o\pi^o \quad ,
\end{aligned}
\tag{4}
$$

$$
\begin{aligned}
K^+n &\rightarrow K^+n\pi^+\pi^- \\
&\rightarrow K^op\pi^+\pi^- \\
&\rightarrow K^on\pi^+\pi^o \\
&\rightarrow K^+p\pi^-\pi^o \\
&\rightarrow K^+n\pi^o\pi^o \\
&\rightarrow K^op\pi^o\pi^o \quad .
\end{aligned}
\tag{5}
$$

To determine the cross sections for K^+ nucleon interactions from the cross sections for K^+d interactions, the impulse approximation has been used. In this approximation it is assumed that one nucleon in the deuteron is only a spectator to the interaction of the incident K^+ with the other nucleon. In reactions such as $K^+d \rightarrow K^opp$, $K^+d \rightarrow K^opp\pi^o$, and $K^+d \rightarrow K^+pp\pi^-$ with two protons in the final state, the incident K^+ must necessarily have interacted with the neutron; and, for these reactions, the K^+d cross sections give a slightly distorted picture of the corresponding free-neutron cross sections. In contrast, the $K^opn\pi^+$ final state can come from the interaction of the K^+ with either of the target nucleons. Fortunately the extremely low momenta anticipated for the spectator nucleons provide a convenient procedure for

choosing which nucleon is the target. This is illustrated in fig. 3 which shows the correlation between neutron and proton momenta for the $K^o\pi^+pn$ final state at 1210 MeV/c. The very low momentum grouping for the protons is a consequence of fitting with an assumed zero momentum, and, in reality, represents a smooth distribution of momenta below 80 MeV/c. Figure 3 indicates that most spectators have momenta below 150 MeV/c whereas practically all recoil nucleons have momenta much in excess of that value. Consequently we have chosen to calculate the ratio of neutron to proton spectators by taking the ratio of events with a neutron of momentum less than 150 MeV/c to those with a proton of momentum less than 150 MeV/c. We have distributed events with both nucleon momenta above 150 MeV/c according to the same ratio.

Figure 1b and table 2 show the division of the $K^+d \rightarrow K^opn\pi^+$ cross section, with the spectator nucleon indicated by parentheses. Also shown in fig. 1b are the $K^+d \rightarrow K^od\pi^+$ cross sections which appear to be flat over the energy range covered by this experiment and the previously published $K^+p \rightarrow K^o\pi^+p$ cross section [3].

The difference between the $K^+p \rightarrow K^o\pi^+p$ and $K^+p(n) \rightarrow K^o\pi^+p(n)$ cross sections is small and is consistent with a rough calculation of the effect of eclipsing and motion of nucleons within the deuteron [5]. If we define the ratio R_c by the relation

$$R_c = \frac{\sigma(K^+p \rightarrow K^o\pi^+p)}{\sigma(K^+d \rightarrow K^o\pi^+p(n))} \quad , \qquad (6)$$

the values of R_c are 1.14±0.14, 1.28±0.11, 1.07±0.06, 1.12±0.10, and 1.14±0.12 at 865, 970, 1210, 1365, and 1585 MeV/c respectively.

We have assumed that the same ratios R_c were applicable in relating the cross sections for $K^+n \rightarrow K^o\pi^+n$, $K^+\pi^-p$, $K^o\pi^op$ to those for $K^+d \rightarrow K^o\pi^+n(p)$, $K^+\pi^-pp$, $K^o\pi^opp$ respectively. The resulting K^+n cross sections are shown in

table 3. Although it is not strictly valid to apply to one channel the free-to-bound-nucleon cross-section ratios found in another, the errors are large enough to encompass channel-to-channel variations, and are propagated in the answers.

Following the procedure of Hirata et al. [6] one can determine the isospin-0 single-pion cross section from the formula,

$$\sigma_0(KN\pi) = 3[\sigma(K^+n \to K^0\pi^+n) + \sigma(K^+n \to K^+\pi^-p) - \sigma(K^+p \to K^+\pi^0p)] \quad , \qquad (7)$$

in which only three of the seven $KN \to KN\pi$ cross sections appear. The $K^+p \to K^+\pi^0p$ cross section has been measured by Bland et al. at the lower four momenta [3] and can be obtained at 1585 MeV/c by interpolation of other published data [10].

The values of $\sigma_0(KN\pi)$ calculated from (7) are shown in table 3 and plotted in fig. 4. We also display in fig. 4 two unfoldings of the total $I = 0$ cross section calculated by Cool et al. [11]. These different unfoldings reflect the variations between different measurements of the K^+d total cross sections in the momentum range between 700 and 1000 MeV/c.* The elastic cross section $\sigma_0(KN)$ also shown in fig. 4 was obtained by subtracting the curve for $\sigma_0(KN\pi)$ from the unfolded total cross section. We were unable to extract reliable values of $\sigma_0(KN\pi\pi)$, but even at 1585 MeV/c $\sigma_0(KN)$ would be only slightly reduced by taking account of the two-pion process.

The rapid increase of $\sigma_0(KN\pi)$ comes near the threshold for the quasi-two-body reaction $KN \to K^*N$. Its onset occurs at a slightly higher momentum than the similar rise of $\sigma_1(KN\pi)$. This is reasonable, because the reaction

*The structure in σ_0(total) near 700 MeV/c reflects in part the fact that the K^+p total cross section as measured by Bugg et al. [1] and Jenkins et al. [7] appears to drop sharply with increasing momentum in that energy region. Recent data from the Rutherford High Energy Laboratory reported by G. Manning at the Pasadena Hadron Physics at Intermediate Energies Conference do <u>not</u> show this drop in the K^+p cross section.

$KN \rightarrow K\Delta$, for which the threshold is somewhat lower and which is known to contribute a major part of $\sigma_1(KN\pi)$ in this region, is forbidden to the isospin-0 channel. Indeed comparison of $\sigma_0(KN\pi)$ with data on $\sigma_1(KN\pi)$ shows that these two cross sections quickly become remarkably similar in magnitude and shape. The rapid increase of $\sigma_0(KN\pi)$ is accompanied by a turnover of $\sigma_0(KN)$. While $\sigma_0(KN)$ falls off more rapidly than $\sigma_1(KN)$, its decrease is no faster than that of the kinematic factor $4\pi\lambda^2$ where λ is the reduced wavelength in the KN center-of-mass system.

As in the case of the isospin-1 K^+N system, it appears that the structure around 1200 MeV/c in the total cross section for the isospin-0 K^+N system is well reconstructed by the sum of three structureless channel cross sections $\sigma_0(KN)$, $\sigma_0(KN\pi)$, and $\sigma_0(KN\pi\pi)$. On the other hand, the low energy behavior of the total elastic isospin-0 cross section is intriguing. $\sigma_0(KN)$ rises rather rapidly from 0 up to about 20 mb around 800 MeV/c at which point it turns over and falls roughly as $4\pi\lambda^2$. Abrams et al. [12] and also J. Dowell [13] have suggested that this peak in $\sigma_0(KN)$ might be due to the existence of a Z_0^* with $M(KN) \sim 1780$ MeV and $\Gamma \sim 565$ MeV. The conclusive establishment of the existence or nonexistence of this Z^* will have to wait until a reliable phase shift analysis is performed in the isospin-0 K^+N system in this region. Some information can be extracted from charge-exchange angular distributions and is discussed in a separate paper [4], but an unambiguous phase shift analysis will require polarization measurements in both the K^0pp and the K^+np final states.

4. SINGLE-PION PRODUCTION

We now consider in more detail the single-pion-production reactions measured in this experiment:

$$K^+d = K^+p(n) \rightarrow K^o\pi^+p(n) \quad (8a)$$

$$K^+n(p) \rightarrow K^o\pi^+n(p) \quad (8b)$$

$$K^+n(p) \rightarrow K^+\pi^-p(p) \quad (8c)$$

$$K^+n(p) \rightarrow K^o\pi^op(p) \quad (8d)$$

where we designate the (slower) spectator nucleon by enclosing it within parentheses. The emphasis of our analysis will be on the isospin-0 $KN \rightarrow K\pi N$ channel. Our results show that above the K^*N threshold at 1080 MeV/c most of the isospin-0 $K\pi N$ production proceeds via the K^*N channel and that the main production mechanism is t-channel pion exchange.

In this analysis we assign $K^+d \rightarrow K\pi NN$ events to $KN \rightarrow K\pi N$ channels by following the procedure discussed in section 3 and discarding events for which the laboratory momentum of both nucleons is greater than 150 MeV/c. To get an empirical measure of the effects of a spectator nucleon we compare measurements of a K^+p reaction with a free proton and with a proton bound in deuterium. As an example we compare in fig. 5 the shapes of various distributions for the reaction $K^+p \rightarrow K^o\pi^+p$ at 1210 MeV/c, measured by Bland et al. [3], with those we obtain for that reaction from $K^+p(n) \rightarrow K^o\pi^+p(n)$ events. Areas of histograms being compared are equal. Figures 5a and 5b compare the $K^o\pi^+$ and $p\pi^+$ invariant mass spectra. Figures 5c,d,e compare production and decay angular distributions for events around the K^* peak, with $K\pi$ mass between 840 and 940 MeV, treating them as $KN \rightarrow K^*N$ with no attempt to subtract out Δ events. Cosine θ is the K^* production-angle cosine $\hat{K}^+\cdot\hat{K}^*$ in the K^*N center of mass, cos α is the polar-decay-angle cosine $\hat{K}^+\cdot\hat{K}^o$ in the K^* center of mass and φ is the Treiman-Yang azimuthal decay angle. Nowhere is there any evidence of distortion of the $K^+p(n) \rightarrow K^o\pi^+p(n)$ distributions. The overall confidence level that the two sets of measurements are compatible is 85%. Similar results are obtained at other momenta. Because

the agreement is good, we assume that the shapes of distributions for other $KN \rightarrow K\pi N$ reactions are likewise not significantly distorted by the presence of a spectator nucleon. The K^* peak in the reaction $K^+p \rightarrow K^o\pi^+p$ is heavily contaminated with $\Delta(1236)$ events because both the Δ-production cross section and the area of the Dalitz plot common to K^* and Δ bands are large. As far as looking for distortions is concerned, it does not matter whether the events are K^* events or not. However the angular distributions shown in fig. 5 are similar to those obtained when a more careful selection of K^* is made, and hence may be used for the qualitative comparison with the K^* angular distributions in the isospin-0 channel given below.

4.1. Resonance Production Cross Sections

Having shown that we can meaningfully assign $K^+d \rightarrow K\pi N(N)$ events to $K^+N \rightarrow K\pi N$ reactions we proceed to determine the resonance production cross sections for the four channels (8a) to (8d). At our energies the dominant final states are

$$K^+N \rightarrow K^*N \qquad (9a)$$

$$\rightarrow K\Delta \qquad (9b)$$

$$\rightarrow K\pi N \text{ nonresonant.} \qquad (9c)$$

The Δ can only be produced from an isospin-1 KN initial state.

The Dalitz plots for reactions (8a-d) at our five momenta are shown in fig. 6. The two lower momenta, 865 and 970, are below the K^* threshold, and exhibit only processes (9b) and (9c), whereas at 1210, 1365, and 1585 MeV/c a considerable amount of K^* is produced.

Because of the increase in complexity above K^* threshold, it is convenient in this discussion to consider separately the data at the two lower momenta from the data at the three higher momenta.

4.1.1. Resonance Production at 865 and 970 MeV/c

The $N\pi$ mass spectra in reactions (8a-d) were fitted to a superposition of three-body phase space and $K\Delta$ production by the same method as described in ref. [3]. The experimental histograms and fitted curves are shown in figs. 7a-d. Free-nucleon cross sections were obtained by scaling the $K^+d \rightarrow K\pi N(N)$ cross section by the ratio R_c defined by eq. (6). The results are in satisfactory agreement with cross sections obtained at these momenta from the analysis of the reaction $K^+p \rightarrow K^o p\pi^+$ in hydrogen by Bland et al. [3] with appropriate application of Clebsch-Gordan coefficients to obtain predictions for the other final states [5].

4.1.2. Resonance Production at 1210, 1365, and 1585 MeV/c

In order to obtain what we believe to be the most reliable measure of K^* production, we have fitted reactions (8a-d) to a superposition of phase space, $K\Delta$ production, NK^* production and $K\Delta$-NK^* interference. In order to reduce the uncertainties somewhat we have constrained the $K\Delta$ cross sections to be those obtained from the $K^+p \rightarrow K^o p\pi^+$ reaction [3] corrected with the Clebsch-Gordan coefficients appropriate to an isospin-1 final state. The fits were made using the empirical interference model of Bland et al. [3], and both data and fitted curves are shown in figs. 7a-d. The resulting K^*p and K^*n cross sections are given in table 4. We have also attempted fits without constraining the $K\Delta$ final states; the results are, within the errors, compatible with those in table 4 [5]. We further note that fits which omit the interference term between NK^* and $K\Delta$ production tend to give very poor χ^2 values. Figure 8 shows the momentum dependence of the K^* production cross sections for the three reactions,

$$K^+p \rightarrow K^{*+}p \qquad (10a)$$

$$K^+n \rightarrow K^{*+}n \qquad (10b)$$

$$K^+n \rightarrow K^{*o}p \quad . \qquad (10c)$$

The K^+n points at 2.3 GeV/c are from S. Goldhaber et al. [14], and the points at 3.0 GeV/c are from Bassompierre et al. [15]. The K^+p points are from Bland et al. [3], S. Goldhaber et al. [16], Bomse et al. [16], and Ferro-Luzzi et al. [16]. For all three reactions the K^* cross sections have roughly the same shapes rising rapidly from threshold until about 1.6 GeV/c, at which point they turn over and fall smoothly. It is of interest to note that

$$\sigma(K^+n \to K^{*o}p) \sim 1.3\ \sigma(K^+p \to K^{*+}p) \sim 2.5\ \sigma(K^+n \to K^{*+}n)$$

from threshold to 3.0 GeV/c.

4.2. K^* Production From the $I = 0$ KN State

4.2.1. Methods

Two different procedures have been used to extract the $I = 0$ K^* production cross section and angular distributions.

(a) Since eq. (7) applies to differential distributions such as angular distributions and invariant-mass spectra, the K^*N cross section can be obtained by making the appropriate fit to the $I = 0$ $K\pi$ mass distribution. Similarly, with an appropriate $K\pi$ mass cut, the $I = 0$ angular distributions can be studied.

(b) Alternatively, the K^*N cross section can be determined from

$$\sigma_o(KN \to K^*N) = 3[\sigma(K^+n \to K^{*+}n \to K^o\pi^+n) + \sigma(K^+n \to K^{*o}p \to K^+\pi^-p) - \frac{1}{2}\sigma(K^+p \to K^{*+}p \to K^o\pi^+p)] \quad , \qquad (11)$$

in which each appropriate deuterium channel is individually separated into K^*N, and the $K^o\pi^+p$ hydrogen channel rather than the $K^+\pi^op$ state is used to subtract out the isospin-1 $K^{*+}p$ part of the cross section.

For the 865, 970, 1210 and 1365 MeV/c data we have used the procedure (a) because it appears less sensitive to the validity of the model used for fitting. This follows from the fact that the combination of eq. (7) eliminates

the Δ contribution completely. At 1585 MeV/c the availability of only the $K^o\pi^+p$ final state in hydrogen permitted only procedure (b) so that the results are perhaps slightly less reliable.

4.2.2. Results

As an example of the procedure we show in fig. 9 the invariant mass spectra for the isospin-0 $KN \rightarrow K\pi N$ channel at 1210 MeV/c together with the corresponding distributions for the three channels $K^+n \rightarrow K^o\pi^+n$, $K^+n \rightarrow K^+\pi^-p$, and $K^+p \rightarrow K^+\pi^o p$ which are the components of $\sigma_o(KN \rightarrow K\pi N)$. Figures 10, 11, 12 show in similar fashion the isospin-0 K^* production and decay angular distributions at 1210, 1365, and 1585 MeV/c together with the component distributions used to construct the $I = 0$ state. The K^* events are taken as those events whose $K\pi$ invariant mass lie in a band from 840 to 940 MeV; no attempt has been made to correct for non-K^* background events included in this band. The angles are defined just as for fig. 5.

The angular distributions shown in figs. 10-12 can be used to study qualitatively the production mechanisms for the three reactions (10a-c). In the $K^+n \rightarrow K^{*o}p \rightarrow K^+\pi^-p$ channel, the production angular distributions peak sharply in the forward direction, the polar decay angular distributions have a large $\cos^2 \alpha$ component, and the azimuthal decay (Treiman-Yang) angular distributions are essentially flat. In the isospin-1 channel, $K^+p \rightarrow K^{*+}p \rightarrow K^o\pi^+p$, the production angular distributions are less sharply peaked, the polar decay distributions vary roughly as $\sin^2 \alpha$, and the azimuthal decay distributions have a $\sin^2 \varphi$ dependence. This behavior has previously been observed at 2.3 [14] and 3.0 GeV/c [15], and was interpreted as indicating that the reaction $K^+p \rightarrow K^{*+}p$ goes predominantly via ω-exchange whereas the reaction $K^+n \rightarrow K^{*o}p$ goes predominantly via pion exchange. The angular distributions for the remaining reaction, $K^+n \rightarrow K^{*+}n \rightarrow K^o\pi^+n$, appear to be

intermediate between those for the other two reactions with no single process appearing to dominate. The most remarkable result is the fact that the $I = 0$ channel shows the clearest pion exchange behavior with the least contamination from vector exchanges. It suggests that the linear combination (7) just happens to cancel out contributions from vector exchanges leaving only the pseudoscalar exchange contribution.

Figure 13 shows the $K\pi$ and $N\pi$ invariant mass spectra in the isospin-0 $KN \rightarrow K\pi N$ channel for momenta at 970, 1210, and 1365 MeV/c; the corresponding spectra at 865 MeV/c are similar to those at 970 MeV/c and those at 1585 MeV/c are inaccessible because of the absence of data on $K^+p \rightarrow K^+\pi^0p$ at that momentum. There is no significant structure in the $N\pi$ spectra which shows that the procedure (7) is successful in eliminating the $\Delta(1238)$ contribution as expected. The K^* peak dominates the $K\pi$ spectrum at momenta above the K^*N threshold. Fits of the $K\pi$ spectrum to phase space and a P-wave Breit-Wigner resonance form having mass 891 MeV and width 50 MeV are shown.

The total isospin-0 $KN \rightarrow K^*N$ cross sections determined as described above are listed in table 4. They can be compared to the corresponding isospin-1 cross sections obtained directly from the $K^+p \rightarrow K^{*+}p$ channel also listed in table 4. Figure 14 shows the energy dependence of the isospin-0 and isospin-1 $KN \rightarrow K^*N$ cross sections from threshold to 3.0 GeV/c. A smooth curve has been drawn through the isospin-1 $KN \rightarrow K^*N$ cross sections and scaled upward by a factor of 3 to give the smooth curve passing through the isospin-0 $KN \rightarrow K^*N$ points. Thus the energy dependences of the isospin-0 and isospin-1 $KN \rightarrow K^*N$ cross sections appear to be similar in shape although differing in magnitude in this energy region. It is perhaps amusing to note that roughly,

$$\sigma_0(K^*N) \approx \sigma_1(K^*N) + \sigma_1(K\Delta) \quad ;$$

that is, the total quasi-two-body cross section is nearly the same for isospin-0 as for isospin-1. The absence of $K\Delta$ for $I = 0$ is compensated by a much larger K^*N cross section. Figure 15 shows the isospin-0 K^* differential cross section, $d\sigma/dt$, together with the density matrix elements (Jackson-frame) ρ_{00}, ρ_{1-1}, and Re ρ_{10}. The differential cross section can be fitted to an exponential

$$d\sigma/dt \sim \exp(bt) \tag{12}$$

with $b = 5.3\pm0.4\ (\mathrm{GeV/c})^{-2}$ at 1210 MeV/c, $b = 4.7\pm0.6\ (\mathrm{GeV/c})^{-2}$ at 1365 MeV/c and $b = 4.8\pm0.6\ (\mathrm{GeV/c})^{-2}$ at 1585 MeV/c. The rather large value of ρ_{00} is indicative of pseudoscalar meson exchange in agreement with our previous observations.

4.3. Production Mechanisms for the Reaction $KN \to K^*N$

The major features of our experimental observations for the reaction $KN \to K^*N$ are summarized in the second column of table 5. We have attempted to get a consistent description of the above experimental observations in terms of s- and t-channel isospin amplitudes A_I and a_I. A particle exchanged in the t-channel contributes to both isospin states in the s-channel. The $KN \to K^*N$ scattering amplitudes, written alternatively in terms of s- and t-channel isospin amplitudes are:

$$A(K^+p \to K^{*+}p) = A_1 = (a_1 - a_0)/2 \tag{13a}$$

$$A(K^+n \to K^{*+}n) = (A_1 + A_0)/2 = -(a_1 + a_0)/2 \tag{13b}$$

$$A(K^+n \to K^{*o}p) = (A_1 - A_0)/2 = a_1 \quad . \tag{13c}$$

Solving for the s-channel isospin amplitudes, we get

$$A_0 = -(a_0 + 3a_1)/2 \tag{14a}$$

$$A_1 = -(a_0 - a_1)/2 \quad . \tag{14b}$$

If the main processes are the exchanges of low-mass mesons, or their Regge trajectories, then

$$A_0 \approx - [(\eta + \omega) + 3(\pi + \rho)]/2 \tag{15a}$$

$$A_1 \approx - [(\eta + \omega) - (\pi + \rho)]/2 \tag{15b}$$

where the particle symbols stand for their amplitudes.

The charge exchange K^* production requires the exchange of at least one isovector meson. Furthermore the angular distributions indicate that at least one pseudoscalar and one vector meson are exchanged. If only one of each is exchanged, the possible pairs are $\pi\rho$, $\eta\rho$, and $\pi\omega$. Simple predictions follow from eqs. (14a) and (14b). For $\pi\rho$, A_0 and A_1 differ at most by a multiplicative constant giving the same angular distributions in the two pure-isospin channels; for $\eta\rho$, there would be much more vector exchange in A_0 than in A_1; and, for $\pi\omega$, there would be much more pseudoscalar exchange in A_0 than in A_1. Since only the last corresponds to the experimental observations, the main processes in this simple picture are π- and ω-exchange. If these were the only processes, one would expect equal $K^{*+}p$ and $K^{*+}n$ cross sections, pure pion exchange in the $K^{*0}p$ final state, and a mixture of pion and vector exchange in the $I = 0$ final state. None of these predictions are in agreement with the observations summarized in table 5. The addition of one more exchange mechanism -- ρ exchange -- can resolve the discrepancies. A possible minimal set of exchanges is thus $\pi\omega\rho$, so that

$$\begin{aligned} A_0 &\approx - [\omega + 3(\pi + \rho)]/2 \qquad & a_0 &\approx \omega \\ A_1 &\approx - [\omega - (\pi + \rho)]/2 \qquad & a_1 &\approx (\pi + \rho) \quad . \end{aligned} \tag{16}$$

The fact that the isospin-0 K^*N final state appears to exhibit pure pion exchange suggests that the ρ-exchange is present by an amount such that the combination $(\omega + 3\rho)$ in A_0 must practically vanish; i.e., $\rho \approx - \omega/3$.

Assuming no interference between pseudoscalar and vector exchanges, we choose a pion exchange contribution which fits the observed $K^{*+}p/K^{*+}n$ ratio of about 2. This requires

$$|\omega|^2 \approx (9/8)|\pi|^2$$

where $|\omega|^2$, $|\pi|^2$ correspond to averages over all momentum transfers. Having thus defined the relative ω, ρ and π exchange contributions we can check whether the other features summarized earlier are properly predicted by (13) and (16). This comparison, summarized in table 5, indicates good qualitative agreement between the experimental observations and the simple $\pi\rho\omega$ exchange model. It may be noted that all these arguments remain valid if π,ω,ρ is expanded to mean the exchange degenerate pairs (π,B), (ω,f) and (ρ,A_2).

5. TWO-PION PRODUCTION

As is clear from table 2, 1585 MeV/c is the only momentum at which we observe substantial two-pion production. For completeness we indicate in table 6 the breakdown of the two-pion cross section at 1585 MeV/c into various channels. Again there is reasonable agreement between the cross sections for the reactions

$$K^+p \rightarrow K^+\pi^-\pi^+p \quad [3]$$

and

$$K^+p(n) \rightarrow K^+\pi^-\pi^+p(n) \quad .$$

The statistics are too small to warrant a shielding correction to go from deuterium to free nucleon cross sections and the deuterium cross sections with proton (neutron) spectators can be taken as reasonable approximations of the corresponding cross sections on free neutron (proton) targets.

One general feature which appears satisfied by <u>all</u> classes of final states (zero pion, one pion, two pion) is the following. If $\sigma(X^+,p)$ and $\sigma(X^+,n)$ are the cross sections for the reactions,

$$K^+p \rightarrow X^+p$$
$$K^+n \rightarrow X^+n \quad ,$$

respectively, $\sigma(X^+,p) > \sigma(X^+,n)$. This is true for $X^+ \equiv K^+$, $X^+ \equiv K^o\pi^+$, and for $X^+ \equiv K^+\pi^+\pi^-$. Since the K^+p and K^+n total cross sections are very nearly equal while there are more channels open to a singly charged system (K^+n) than to a doubly charged one (K^+p), one might expect on the average to have $\sigma(X^+,p) > \sigma(X^+,n)$, but it is remarkable that this should be true channel by channel.

6. SUMMARY AND CONCLUSIONS

The study of K^+d interactions between 865 and 1585 MeV/c has provided some detailed information concerning the $I = 0$ KN system. The main features observed can be summarized as follows:

(1) There is qualitative similarity between the momentum dependence of $\sigma_o(KN)$, $\sigma_o(KN\pi)$, $\sigma_o(KN\pi\pi)$, and that of $\sigma_1(KN)$, $\sigma_1(KN\pi)$ and $\sigma_1(KN\pi\pi)$. The main differences are that the dropoff in $\sigma_o(KN)$ above 1 GeV/c is much steeper than for $\sigma_1(KN)$, and the sharp rise in $\sigma_o(KN\pi)$ occurs at a slightly higher momentum than for $\sigma_1(KN\pi)$. Just as in the case of the isospin-1 channel, the total cross section maximum near 1150 MeV/c for the isospin-0 channel arises from the combination of a dropping elastic cross section and a rising one-pion cross section.

(2) The $KN\pi$ final state in the isospin-0 channel is dominated by K^* production. Indeed this process has a cross section about three times as large as that for isospin-1 K^* production. This fact accounts for the result that in spite of the absence in the $I = 0$ reaction of the $K\Delta$ final state which dominates the $I = 1$ process, $\sigma_o(KN\pi)$ above K^* threshold has nearly the same value as $\sigma_1(KN\pi)$.

(3) Production and decay angular distributions in the reaction $K^+n \rightarrow K^{*o}p$ exhibit, even within 100 MeV/c of threshold, just the same features as observed at much higher momenta. Specifically the production angular distribution has a sharp forward peak, and the decay correlations are characteristic of pseudoscalar exchange. Surprisingly the pure isospin-0 K^*N final state exhibits these characteristics to an even more marked degree. This observation as well as the relative cross sections for various K^*N charge combinations can be understood by assuming some ρ exchange contribution in addition to the already established π and ω exchange.

(4) There is no experimental evidence that the structure in σ_o(total) at 1150 MeV/c is to be interpreted in terms of a largely inelastic resonance of mass 1865 MeV. The cross section $\sigma_o(KN\pi)$ does not show any bump at this momentum; furthermore the major inelastic channel K^*N is produced in a highly peripheral manner and is not dominated by any one partial wave.

Aaron et al. [17] have suggested on theoretical grounds that the rapidly rising $\sigma_o(K^*N)$ should lead to resonant behavior in incident $S_{1/2}$ and $D_{3/2}$ waves. Their calculated behavior of $\sigma_o(KN\pi)$ is not incompatible with the experimental curve in fig. 4, and they note that even the highly peripheral K^*N production angular distribution observed is not inconsistent with the dominant $S_{1/2}$ state required by their model. Thus one cannot make any conclusive statement about the absence of an inelastic resonance from our data. As emphasized in the qualitative model discussed in section 4.3 the K^*N production can be understood in terms of t-channel processes. From duality considerations, however, this observation also does not rule out the presence of an inelastic resonance at roughly 1900 MeV. We can only say that there is nothing in our experimental observations which demands the existence of an inelastic $Z^*(1900)$.

We express our appreciation to the 25-inch bubble chamber crew and Bevatron staff for their help during the experimental run, to Howard White and the Data Handling Group, and to Dr. Roger Bland and Mrs. Bronwyn Hall for helpful discussions. We also gratefully acknowledge the efforts of our scanning, measuring, and programming staff.

REFERENCES

[1] R. L. Cool, G. Giacomelli, T. F. Kycia, B. A. Leontic, K. K. Li, A. Lundby, J. Teiger, and C. Wilkin, Phys. Rev. D1 (1970) 1887;

D. V. Bugg, R. S. Gilmore, K. M. Knight, D. C. Salter, G. H. Stafford, E. J. N. Wilson, J. D. Davies, J. D. Dowell, P. M. Hattersley, R. J. Homer, A. W. O'Dell, A. A. Carter, R. J. Tapper, and K. F. Riley, Phys. Rev. 168 (1968) 1466.

[2] R. Ayed, P. Bareyre, J. Feltesse, and G. Villet, Phys. Letters 32B (1970) 404;

P. C. Barber, T. A. Broome, B. G. Duff, F. F. Heymann, D. C. Imrie, G. J. Lush, B. R. Martin, K. M. Potter, D. M. Ritson, L. A. Robbins, R. A. Rosner, S. J. Sharrock, A. D. Smith, R. C. Hanna, A. T. Lea, and E. J. Sacharides, Phys. Letters 32B (1970) 214;

G. Giacomelli, P. Lugaresi-Serra, G. Mondrioli, A. M. Rossi, F. Griffiths, I. S. Hughes, D. A. Jacobs, R. Jennings, B. C. Wilson, G. Ciapetti, V. Castantini, G. Martellotti, D. Zanello, E. Castelli, and M. Sessa, Nucl. Phys. B20 (1970) 301;

S. Kato, P. Koehler, T. Novey, A. Yokosawa, and G. Burleson, Phys. Rev. Letters 24 (1970) 615;

C. Lovelace and F. Wagner, CERN Report Th-1251 (1970);

G. A. Rebka, J. Rothberg, A. Etkin, P. Glodis, J. Greenberg, V. W. Hughes, K. Kondo, D. C. Lu, J. Mori, and P. A. Thompson, Phys. Rev. Lett. 24 (1970) 160;

see also Hyperon Resonances - 70, edited by E. C. Fowler (Moore Publishing Company, Durham, North Carolina, 1970), pp. 349-461.

[3] R. W. Bland, M. G. Bowler, J. L. Brown, J. A. Kadyk, G. Goldhaber, S. Goldhaber, J. A. Kadyk, V. H. Seeger, and G. H. Trilling, Nucl. Phys. B13 (1969) 595;
R. W. Bland, M. G. Bowler, J. L. Brown, G. Goldhaber, S. Goldhaber, J. A. Kadyk, V. H. Seeger, and G. H. Trilling, Nucl. Phys. B18 (1970) 537.

[4] A. A. Hirata, G. Goldhaber, B. H. Hall, V. H. Seeger, G. H. Trilling, and C. G. Wohl, UCRL-20243, Nucl. Phys. B (in press).

[5] More detailed discussions are given in the Ph.D. theses of A. A. Hirata, Lawrence Radiation Laboratory Report UCRL-20248 (1970), and V. H. Seeger, UCRL-20628 (1971).

[6] A. A. Hirata, C. G. Wohl, G. Goldhaber, and G. H. Trilling, Phys. Rev. Letters 21 (1968) 1485; Errata, Phys. Rev. Letters 21 (1968) 1728.

[7] T. Bowen, P. K. Caldwell, F. N. Dikmen, E. W. Jenkins, R. M. Kalbach, D. V. Petersen, and A. E. Pifer, Phys. Rev. D2 (1970) 2599.

[8] W. Slater, D. H. Stork, H. K. Ticho, W. Lee, W. Chinowsky, G. Goldhaber, S. Goldhaber, and T. O'Halloran, Phys. Rev. Letters 7 (1961) 378.

[9] I. Butterworth, J. L. Brown, G. Goldhaber, S. Goldhaber, A. A. Hirata, J. A. Kadyk, B. M. Schwarzschild, and G. H. Trilling, Phys. Rev. Letters 15 (1965) 734, and unpublished data of the same authors.

[10] A. Bettini, M. Cresti, S. Limentani, L. Perruzzo, R. Santangelo, D. Locke, D. J. Crennell, W. T. Davies, and P. B. Jones, Phys. Letters 16 (1965) 83; W. Chinowsky, G. Goldhaber, S. Goldhaber, T. O'Halloran, and B. Schwarzschild, Phys. Rev. 139 (1965) B1411.

[11] R. L. Cool, in Hyperon Resonances - 70, edited by E. C. Fowler (Moore Publishing Company, Durham, North Carolina, 1970), p. 47.

[12] R. J. Abrams, R. L. Cool, G. Giacomelli, T. F. Kycia, K. K. Li, and D. N. Michael, Phys. Letters 30B (1969) 564.

[13] J. D. Dowell, in Hyperon Resonances - 70, edited by E. C. Fowler (Moore Publishing Company, Durham, North Carolina, 1970), p. 53.

[14] S. Goldhaber, J. L. Brown, I. Butterworth, G. Goldhaber, A. A. Hirata, J. A. Kadyk, and G. H. Trilling, Phys. Rev. Letters 15 (1965) 737.

[15] G. Bassompierre, Y. Goldschmidt-Clermont, A. Grant, V. P. Henri, B. Jongejans, U. Kundt, F. Muller, J. M. Perreau, H. Piotrowska, R. Sekulin, J. K. Touminiemi, J. M. Crispeels, J. Debaisieux, J. De Jongh, M. Delabaye, P. Dufour, F. Grard, J. Heughebaert, J. Naisse, S. Tarernier, G. Thill, K. Buchner, G. Dehm, G. Goebel, H. Hupe, T. Joldersma, I. S. Mittra, W. Wittek, and G. Wolf, Nucl. Physics B16 (1970) 125.

[16] M. Ferro-Luzzi, R. George, Y. Goldschmidt-Clermont, V. P. Henri, B. Jongejans, D. W. G. Leith, G. R. Lynch, F. Muller, and J. M. Perreau, Nuovo Cimento 36 (1965) 1101;

S. Goldhaber, W. Chinowsky, G. Goldhaber, and T. O'Halloran, Phys. Rev. 142 (1966) 913;

F. Bomse, S. Borenstein, J. Cole, D. Gillespie, R. Kraemer, G. Luste, I. Miller, E. Moses, A. Pevsner, R. Singh, and R. Zdanis, Phys. Rev. 158 (1967) 1298.

[17] R. Aaron, R. D. Amado, and R. R. Silbar, Phys. Rev. Lett. 26 (1971) 407.

Table 1. Numbers of events found in directly measured channels.

Channel	Momentum (MeV/c) 865	970	1210	1365	1585
$K^+ \rightarrow \pi^+\pi^+\pi^-$	570	956	827	377	372
$K^+d \rightarrow K^0pp$	559	996	832	311	245
$K^0pp\pi^0$	39	129	354	177	241
$K^0pn\pi^+$	89	369	1018	505	566
$K^0d\pi^+$	11	20	23	15	12
$K^0d\pi^+\pi^0$	0	0	1	1	9
$K^0NN\pi\pi$ [a]	0	0	3	22	69
$K^+d \rightarrow K^+pp\pi^-$	122	461	1583	894	914
$K^+pp\pi^-\pi^0$	0	0	11	14	93
$K^0pp\pi^-\pi^+$ [b]	0	0	12	23	27
$K^+pn\pi^-\pi^+$	0	2	22	53	125
$K^+d\pi^-\pi^+$	0	0	2	5	4

[a]) Events with two neutral particles in the final state.

[b]) At 1210 and 1365 MeV/c events with or without a vee are used; at 1585 MeV/c only events with a vee are used.

Table 2. K^+d scattering cross sections (in mb).

	Channel	Momentum (MeV/c) 865	970	1210	1365	1585
Cross sections directly measured	$K^+d \to K^0pp$	6.72±0.40	6.26±0.29	4.99±0.24	3.69±0.29	2.57±0.21
	$\to K^0pp\pi^0$	0.48±0.08	0.82±0.08	2.09±0.13	2.06±0.19	2.42±0.20
	$\to K^0pn\pi^+$	1.24±0.14	2.47±0.16	6.21±0.29	6.08±0.42	5.88±0.39
	$\to K^+pp\pi^-$	0.46±0.05	0.91±0.05	2.89±0.12	3.21±0.20	3.76±0.26
	$\to KNN\pi\pi$ [a])	---	0.01±0.005	0.11±0.02	0.59±0.07	1.86±0.15
Components of $K^+d \to K^0pn\pi^+$	$K^+d \to K^0\pi^+d$	0.13±0.04	0.13±0.03	0.14±0.03	0.18±0.05	0.31±0.04
	$K^+p(n) \to K^0\pi^+p(n)$	0.98±0.13	1.99±0.15	4.76±0.26	4.78±0.38	4.37±0.32
	$K^+n(p) \to K^0\pi^+n(p)$	0.13±0.04	0.35±0.05	1.31±0.12	1.12±0.15	1.39±0.14
Derived cross sections [b])	$K^+d \to KNN$	27.59±0.32	27.17±0.35	22.73±0.63	20.97±0.99	17.75±0.84
	$\to K^+pn$	20.87±0.56	20.91±0.50	17.74±0.78	17.28±1.15	15.18±0.87
	$\to KNN\pi$	2.74±0.24	5.54±0.29	14.51±0.60	15.54±0.95	16.30±0.76
	$\to KNN\pi\pi$ [c])	---	0.01±0.005	0.17±0.05	0.76±0.18	2.20±0.36
	K^+d total [d])	30.33±0.21	32.72±0.19	37.41±0.20	37.27±0.15	36.25±0.15

[a]) This is the sum over the six (of eight) charge channels observed.

[b]) These include cross sections for the reactions in which NN is a deuteron.

[c]) This cross section includes all charge channels and is obtained by using isospin relationships as described in Hirata et al. [6].

[d]) From Bugg et al. [1].

Table 3. K^+N one-pion production cross sections (in mb). The errors are statistical only.

Channel [a]	Momentum (MeV/c)				
	865	970	1210	1365	1585
$K^+n \to K^0p\pi^0$	0.55±0.11	1.05±0.14	2.24±0.19	2.31±0.30	2.76±0.36
$\to K^0n\pi^+$	0.15±0.05	0.45±0.07	1.40±0.15	1.25±0.20	1.58±0.16
$\to K^+p\pi^-$	0.52±0.09	1.16±0.12	3.09±0.22	3.60±0.39	4.29±0.53
$(KN \to KN\pi)_{I=0}$	1.0 ±0.4	2.5 ±0.6	8.0 ±0.9	10.1 ±1.7	11.7 ±1.8

[a]) The $K^+n \to KN\pi$ cross sections are the $K^+d \to KN\pi(N)$ cross section measured in deuterium multiplied by the ratio $\sigma(K^+p \to K^0\pi^+p)/\sigma[K^+p(n) \to K^0\pi^+p(n)]$.

Table 4. $KN \rightarrow K^*(891)N$ scattering cross sections (in mb). The errors on cross sections from this experiment are statistical only. All $K^*(891)$ decay modes are included in the cross sections.

Channel	Momentum (MeV/c)		
	1210	1365	1585
$K^+p \rightarrow K^{*+}p$ [a]	1.74±0.23	2.6±0.3	3.2±0.4
$K^+n \rightarrow K^{*+}n$ [b]	1.0±0.2	1.2±0.3	1.2±0.4
$K^+n \rightarrow K^{*0}p$ [c]	2.4±0.2	3.3±0.4	4.2±0.6
$(KN \rightarrow K^*N)_{I=0}$	6.0±0.8 [d]	8.6±1.6 [d]	7.5±1.4 [d]
$(KN \rightarrow K^*N)_{I=1}$	1.74±0.23	2.6±0.3	3.2±0.4

[a]) From Bland et al. [3].

[b]) We have used R (all K^{*+} charge states)/R($K^{*+} \rightarrow K^0\pi^+$) = 3/2.

[c]) We have used R (all K^{*0} charge states)/R ($K^{*0} \rightarrow K^+\pi^-$) = 3/2.

[d]) We have used eq. (7) at 1210 and 1365, and eq. (11) at 1585 MeV/c.

Table 5. Tests of simple $\pi\rho\omega$ exchange model.

Cross-section ratio	Experiment	Model prediction
$\frac{\sigma(K^+p \to K^{*+}p)}{\sigma(K^+n \to K^{*+}n)}$	~ 2	2.0
$\frac{\sigma(K^+n \to K^{*0}p)}{\sigma(K^+p \to K^{*+}p)}$	~ 1.3	1.5
$\frac{\sigma_0(KN \to K^*N)}{\sigma_1(KN \to K^*N)}$	~ 3	3.0

Reaction	Experimental features of angular distribution	model prediction
$(K^*N \to K^*N)_{I=0}$	~ pure π exchange	pure π exchange
$K^+p \to K^{*+}p$	~ dominated by vector exchange	2/3 vector exchange 1/3 π exchange
$K^+n \to K^{*+}n$	no dominant process	1/3 vector exchange 2/3 π exchange
$K^+n \to K^{*0}p$	~ dominated by π exchange	8/9 π exchange 1/9 vector exchange

Table 6. Two-pion production cross sections at 1585 MeV/c.

Channel	Cross section (mb)
$K^+d \rightarrow K^0nn\pi^+\pi^+$	0.11±0.04 [a])
$\rightarrow K^+pn\pi^+\pi^-$	0.52±0.09
$\rightarrow K^0pp\pi^+\pi^-$	0.27±0.05
$\rightarrow K^0pn\pi^+\pi^0$	0.48±0.07 [a])
$\rightarrow K^+pp\pi^-\pi^0$	0.37±0.07
$\rightarrow K^0pp\pi^0\pi^0$	0.10±0.04 [a])
$K^+d \rightarrow KNN\pi\pi$ [b])	2.20±0.36
$K^+d \rightarrow K^+\pi^+\pi^-n(p)$	0.16±0.05
$\rightarrow K^+\pi^+\pi^-p(n)$	0.35±0.07
$\rightarrow K^+\pi^+\pi^-d$	0.01±0.01

[a]) These channels are all unconstrained situations in which the missing mass is greater than appropriate for a single missing neutral. Since three-pion cross sections are negligible, the interpretations given are the only ones possible. Because of the inability to perform a constrained fit, the final state $K^0pn\pi^+\pi^0$ cannot be apportioned among neutrons and proton spectators.

[b]) This cross section is derived using isospin relationships as described in Hirata et al. [6] and is therefore larger than the sum of the six identifiable two-pion channel cross sections.

FIGURE CAPTIONS

Fig. 1. (a) Cross sections for various final states produced in K^+d interactions. (b) Components of the $K^o\pi^+pn$ final state. The cross section for $K^+p \rightarrow K^+\pi^o p$ [3] is shown for comparison.

Fig. 2. Cross sections for K^+d going into various classes of final states as a function of incident momentum. The total cross-section data are from ref. [1] and ref. [7]. Open circles are based on partial cross sections obtained in this experiment whereas solid circles are from data of ref. [8] and ref. [9].

Fig. 3. Scatter plot of neutron versus proton momentum in the reaction $K^+d \rightarrow K^o\pi^+pn$ at 1210 MeV/c.

Fig. 4. Isoscalar KN cross sections as a function of incident momentum. Data for $\sigma_o(KN\pi)$ are from the present experiment except for the two highest points which are from ref. [9] and ref. [15]. σ_o(total) is from the unfolding of Cool et al. [11]. The solid and dashed curves indicate the limits on the total cross section determined by the spread of results from various experiments.

Fig. 5. Comparisons of various distributions for $K^+p \rightarrow K^o\pi^+p$ and $K^+d \rightarrow K^o\pi^+p(n)$ at 1210 MeV/c.

Fig. 6. Dalitz plots for single pion production reactions.

Fig. 7. $K\pi$ and $N\pi$ mass spectra for (a) $K^+d \rightarrow K^o\pi^+p(n)$, (b) $K^+d \rightarrow K^o\pi^+n(p)$, (c) $K^+d \rightarrow K^+\pi^-p(p)$, and (d) $K^+d \rightarrow K^o\pi^o p(p)$. Solid curves are from fits discussed in the text.

Fig. 8. Cross sections for K^*N production as a function of incident momentum.

Fig. 9. $K\pi$ and $N\pi$ mass spectra at 1210 MeV/c for $I = 0$ final state and for the various channels used to construct this state.

Fig. 10. Distributions of $\cos\theta$, $\cos\alpha$ and φ for K^* production in $I = 0$

final state and in channels used to construct this final state. The incident momentum is 1210 MeV/c.

Fig. 11. Distributions of cos θ, cos α and φ for K^* production in $I = 0$ final state and in channels used to construct this final state. The incident momentum is 1365 MeV/c.

Fig. 12. Distributions of cos θ, cos α and φ for K^* production in $I = 0$ final state and in channels used to construct this final state. The incident momentum is 1585 MeV/c.

Fig. 13. Isospin-0 $K\pi$ and $N\pi$ mass spectra.

Fig. 14. Cross sections for isospin-0 and isospin-1 K^*N production. The experimental points include data from refs. [3], [15], and [16].

Fig. 15. Differential cross sections and density matrix elements for isospin-0 K^*N production.

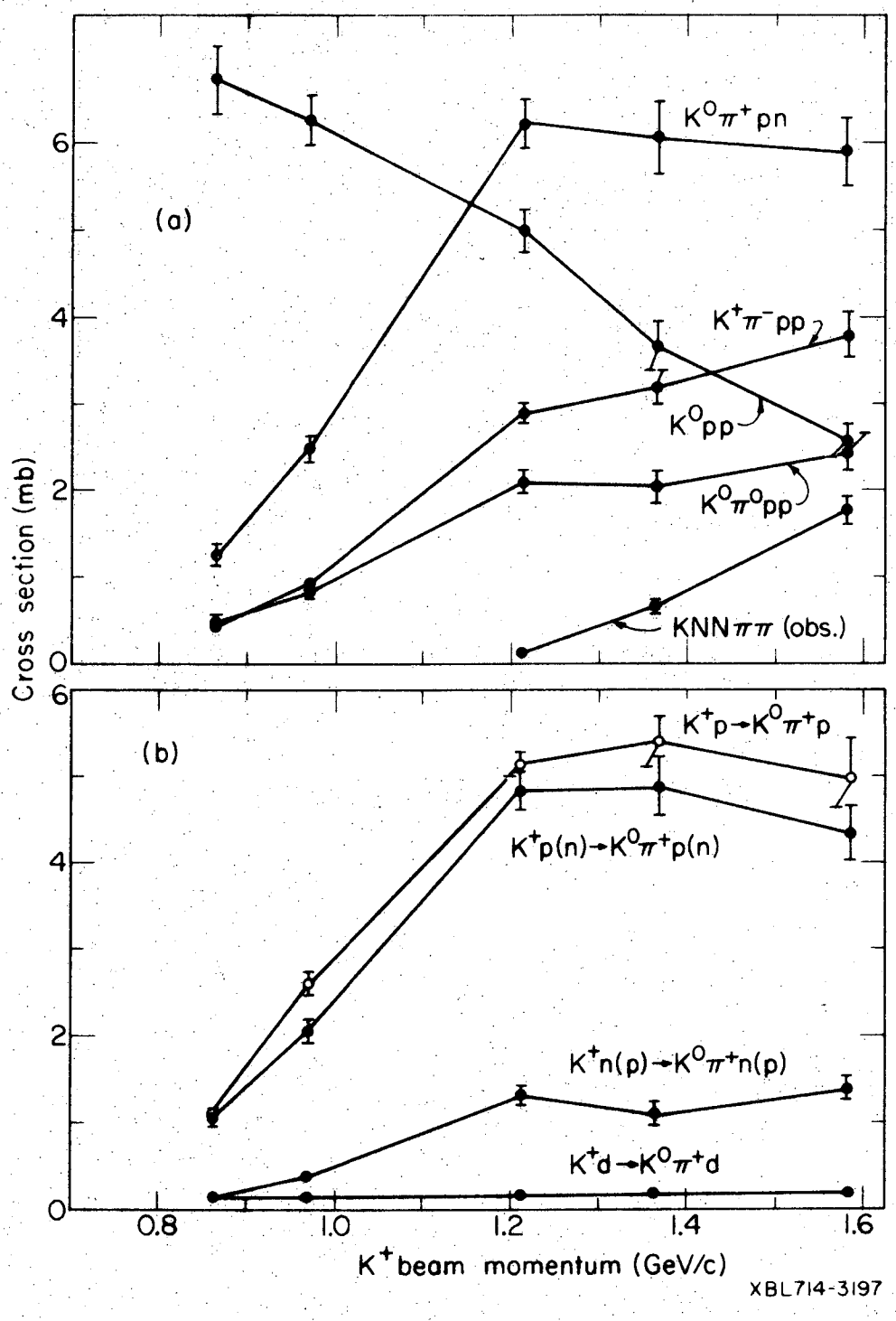
(a)
$K^0\pi^+pn$
$K^+\pi^-pp$
K^0pp
$K^0\pi^0pp$
$KNN\pi\pi$ (obs.)
(b)
$K^+p \to K^0\pi^+p$
$K^+p(n) \to K^0\pi^+p(n)$
$K^+n(p) \to K^0\pi^+n(p)$
$K^+d \to K^0\pi^+d$
Cross section (mb)
0
2
4
6
0.8
1.0
1.2
1.4
1.6
K^+ beam momentum (GeV/c)
XBL714-3197

Fig. 1

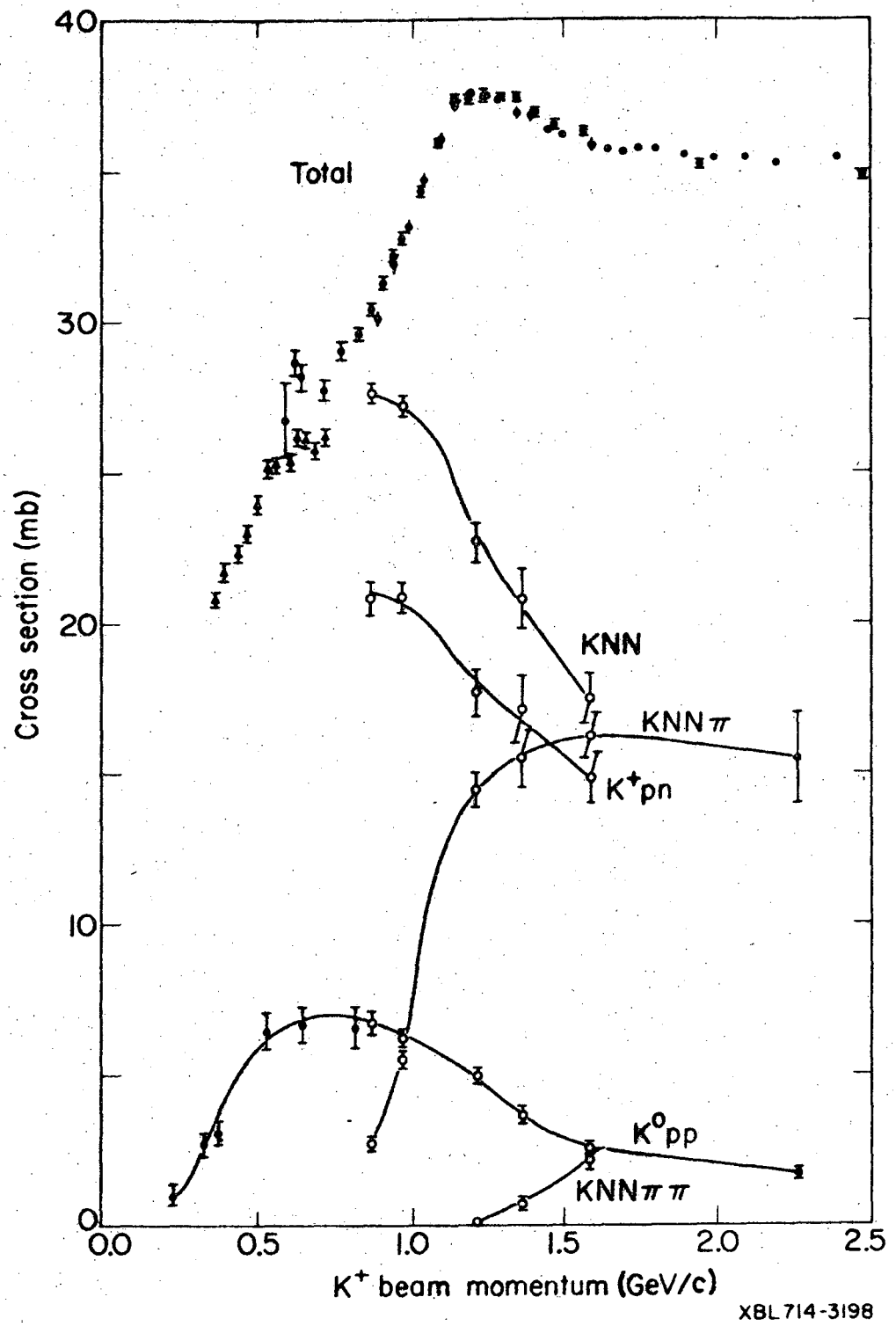
40
30
20
10
0
Cross section (mb)
Total
KNN
KNNπ
K⁺pn
K⁰pp
KNNππ
0.0
0.5
1.0
1.5
2.0
2.5
K⁺ beam momentum (GeV/c)
XBL 714-3198

Fig. 2

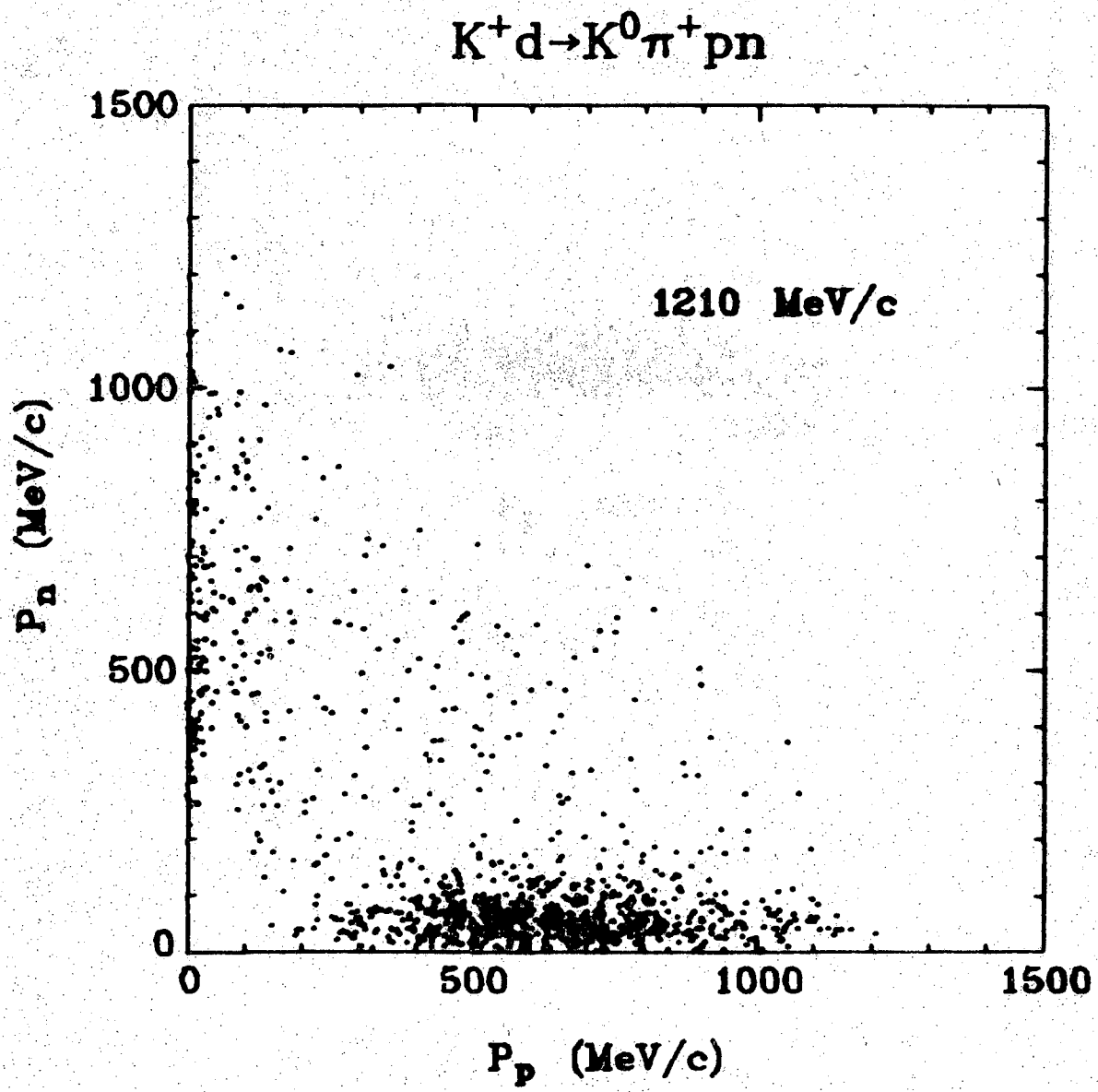

XBL 708-1984

Fig. 3

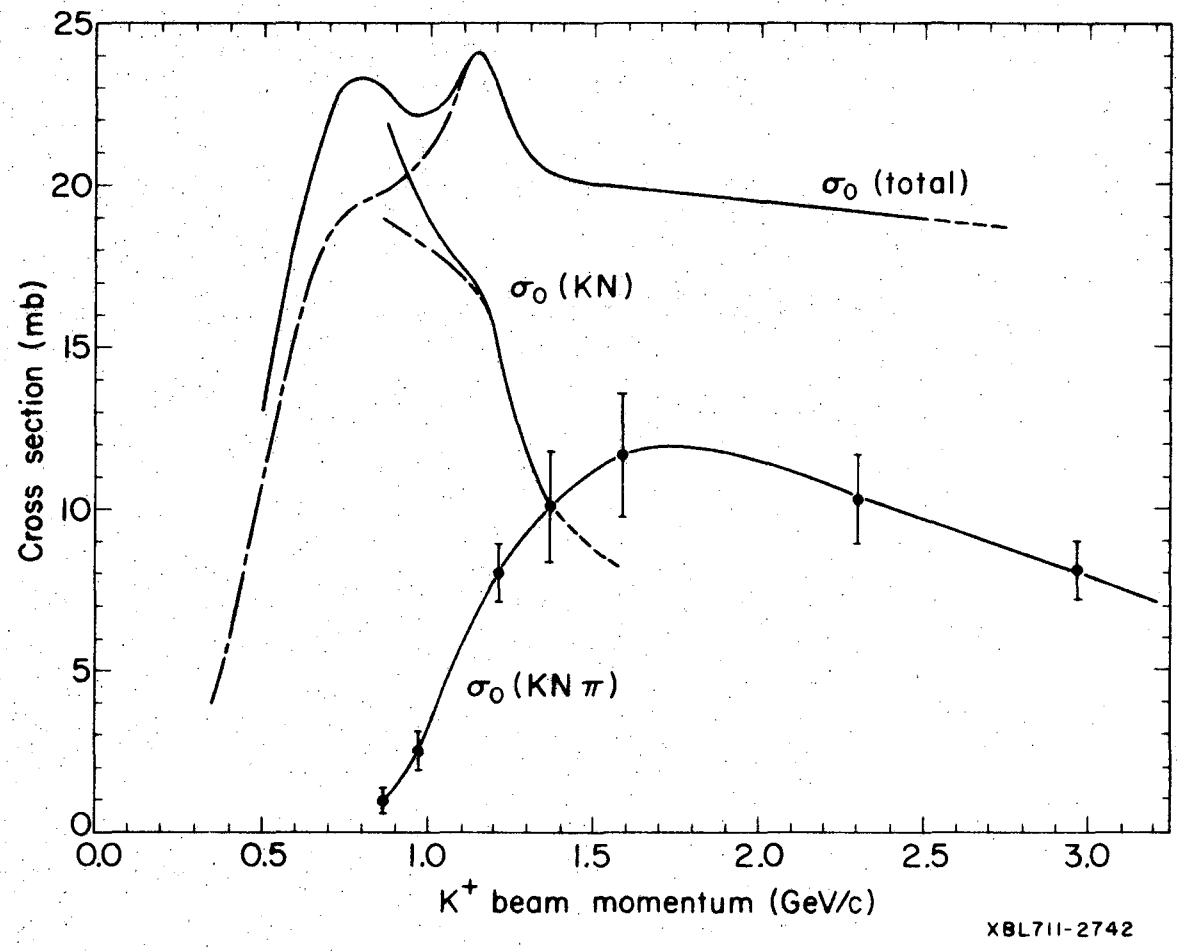
25
20
15
10
5
0
Cross section (mb)
0.0
0.5
1.0
1.5
2.0
2.5
3.0
K+ beam momentum (GeV/c)
σ0 (total)
σ0 (KN)
σ0 (KN π)
XBL711-2742

Fig. 4

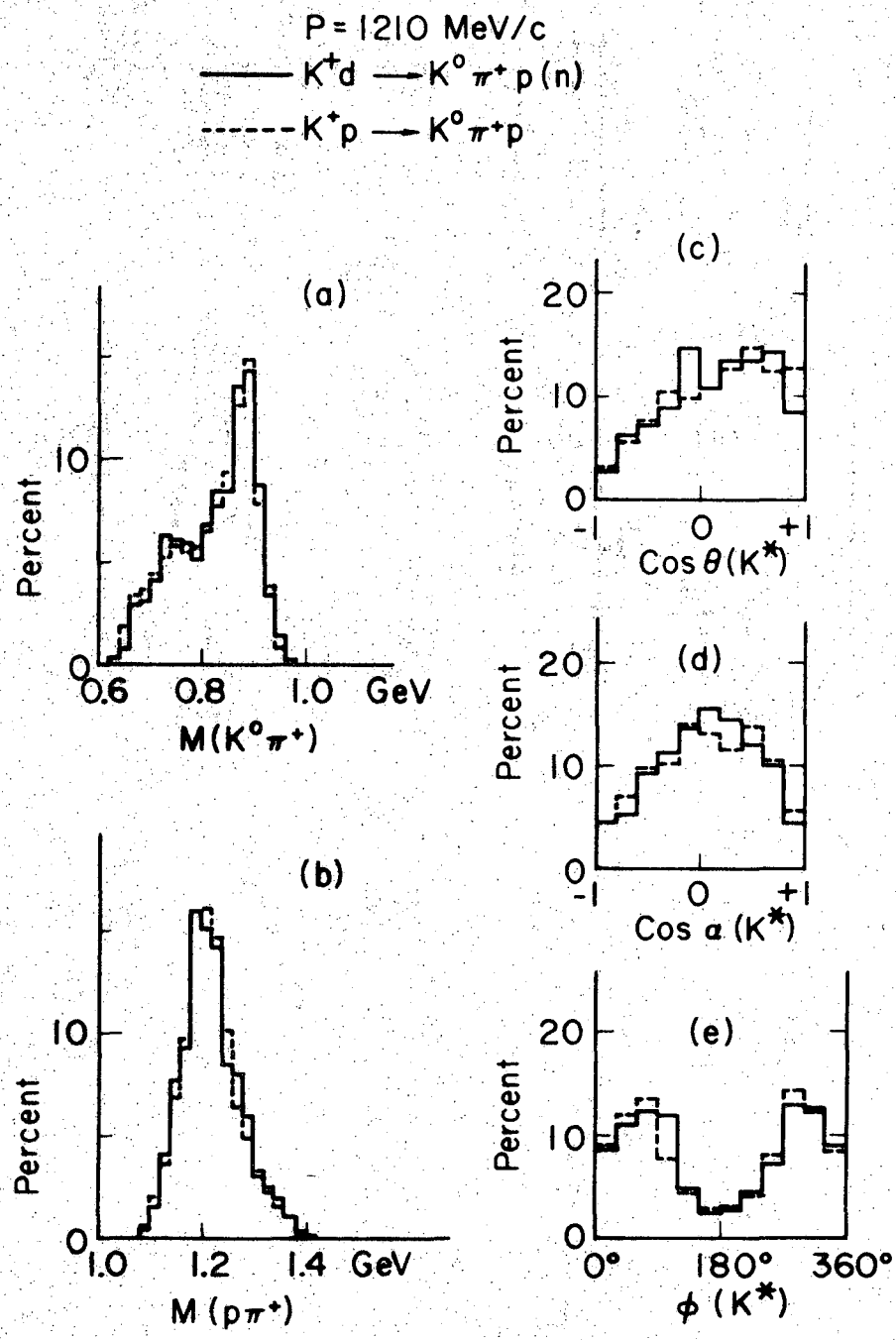
P = 1210 MeV/c
K+d → K0 π+ p (n)
K+p → K0 π+ p
(a)
Percent
10
0
0.6
0.8
1.0
GeV
M(K0 π+)
(b)
Percent
10
0
1.0
1.2
1.4
GeV
M (pπ+)
(c)
Percent
20
10
0
-1
0
+1
Cos θ (K*)
(d)
Percent
20
10
0
-1
0
+1
Cos α (K*)
(e)
Percent
20
10
0
0°
180°
360°
φ (K*)
XBL697-3211

Fig. 5

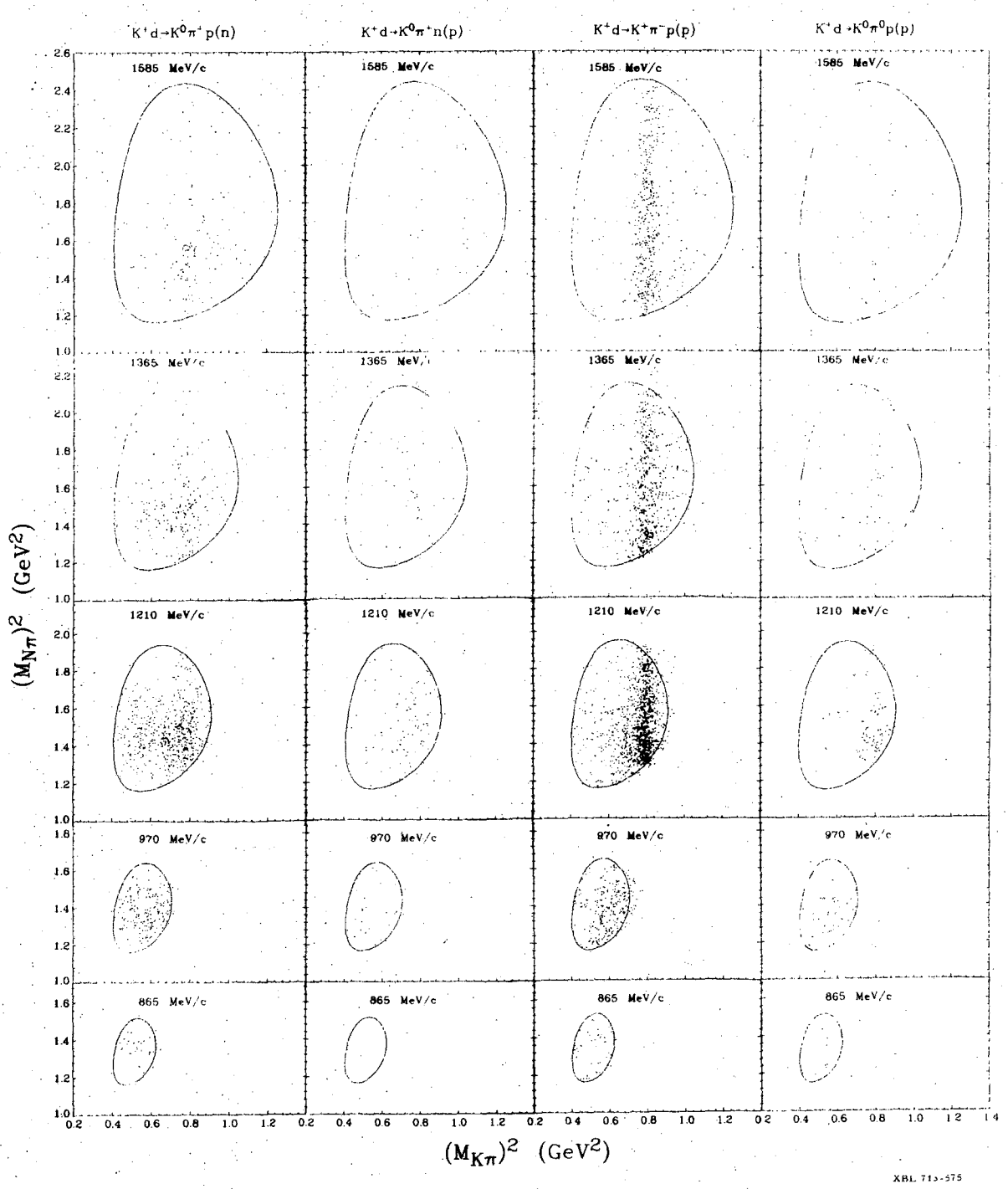
K⁺d→K⁰π⁺p(n)
K⁺d→K⁰π⁺n(p)
K⁺d→K⁺π⁻p(p)
K⁺d→K⁰π⁰p(p)
1585 MeV/c
1365 MeV/c
1210 MeV/c
970 MeV/c
865 MeV/c
(M_Nπ)² (GeV²)
(M_Kπ)² (GeV²)
XBL 713-575

Fig. 6

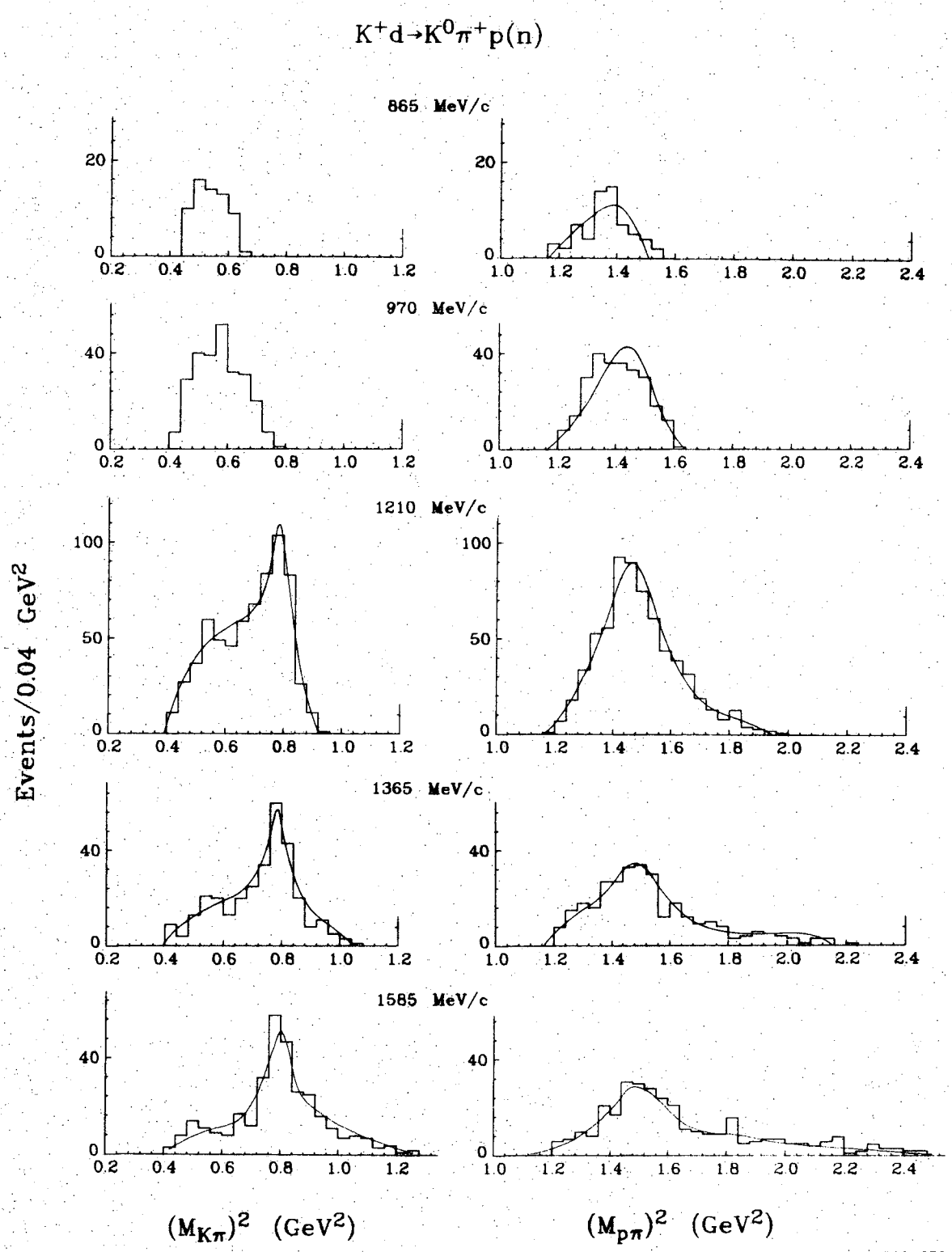
$K^+d \to K^0\pi^+p(n)$
865 MeV/c
970 MeV/c
1210 MeV/c
1365 MeV/c
1585 MeV/c
Events/0.04 GeV^2
$(M_{K\pi})^2$ (GeV^2)
$(M_{p\pi})^2$ (GeV^2)
XBL 713-573

Fig. 7a

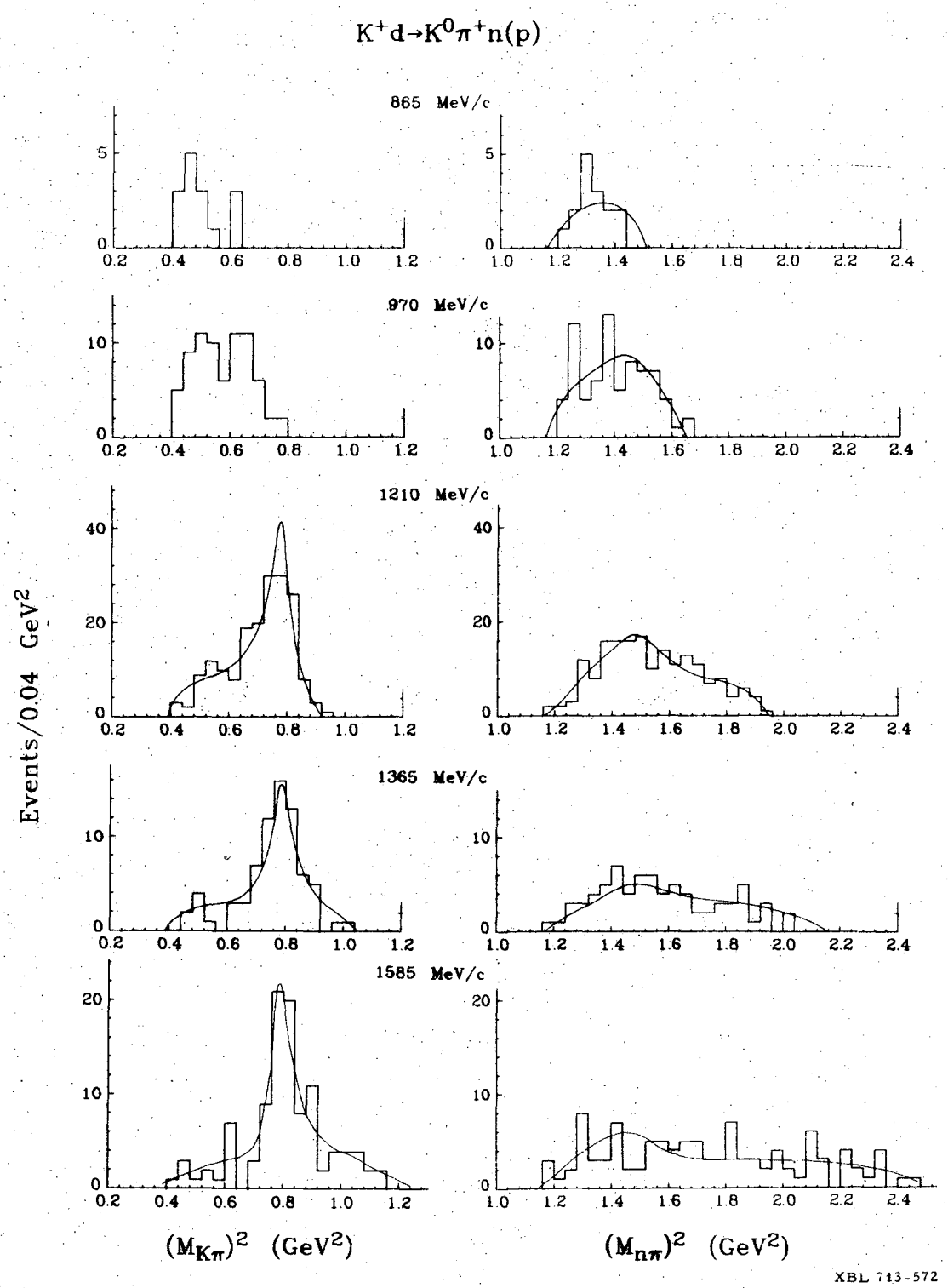
$K^+d \to K^0\pi^+n(p)$
865 MeV/c
970 MeV/c
1210 MeV/c
1365 MeV/c
1585 MeV/c
Events/0.04 GeV^2
$(M_{K\pi})^2$ (GeV^2)
$(M_{n\pi})^2$ (GeV^2)
XBL 713-572

Fig. 7b

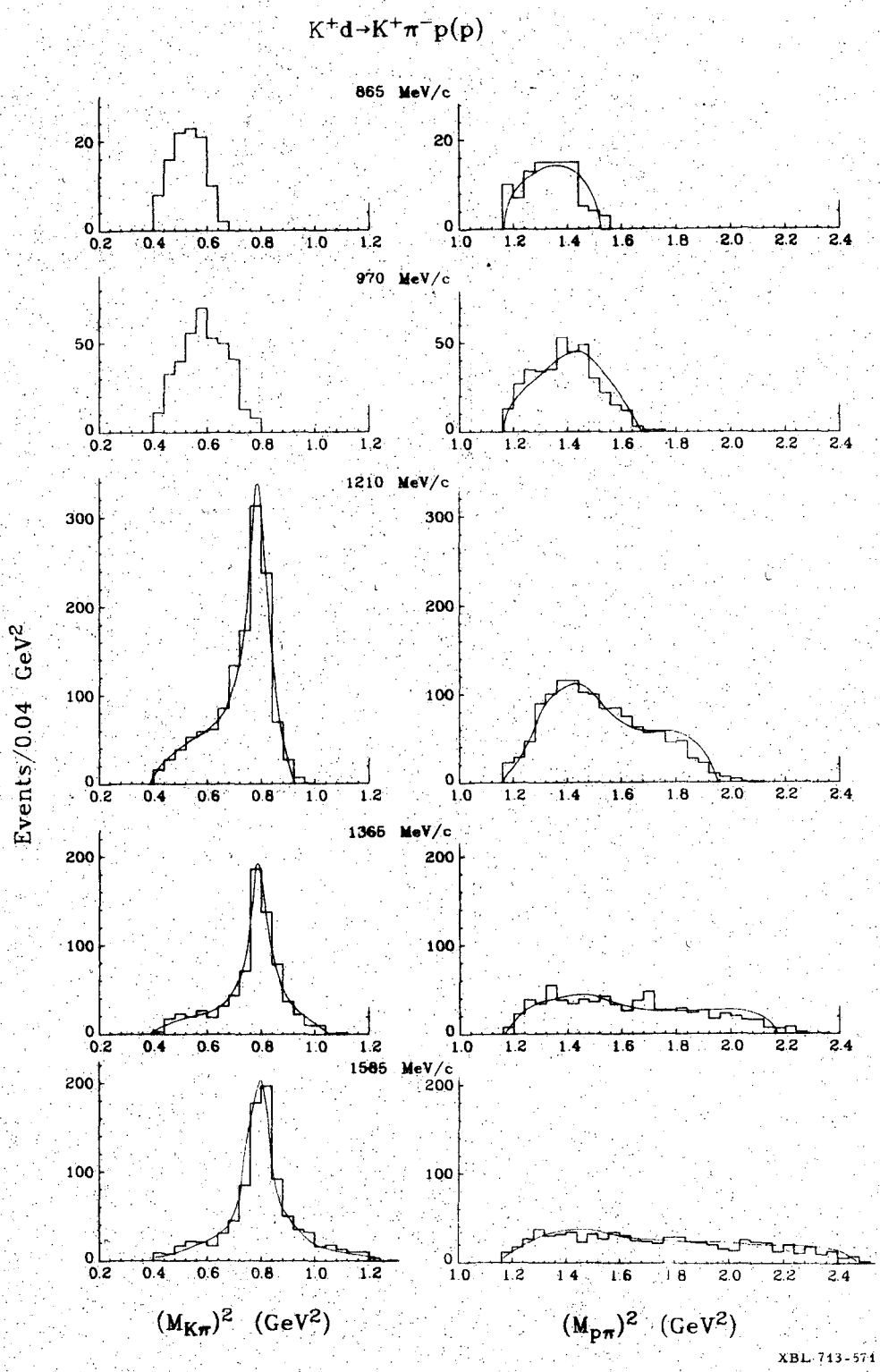
$K^+d \to K^+\pi^-p(p)$
865 MeV/c
970 MeV/c
1210 MeV/c
1365 MeV/c
1585 MeV/c
Events/0.04 GeV^2
$(M_{K\pi})^2$ (GeV^2)
$(M_{p\pi})^2$ (GeV^2)
XBL 713-571

Fig. 7c

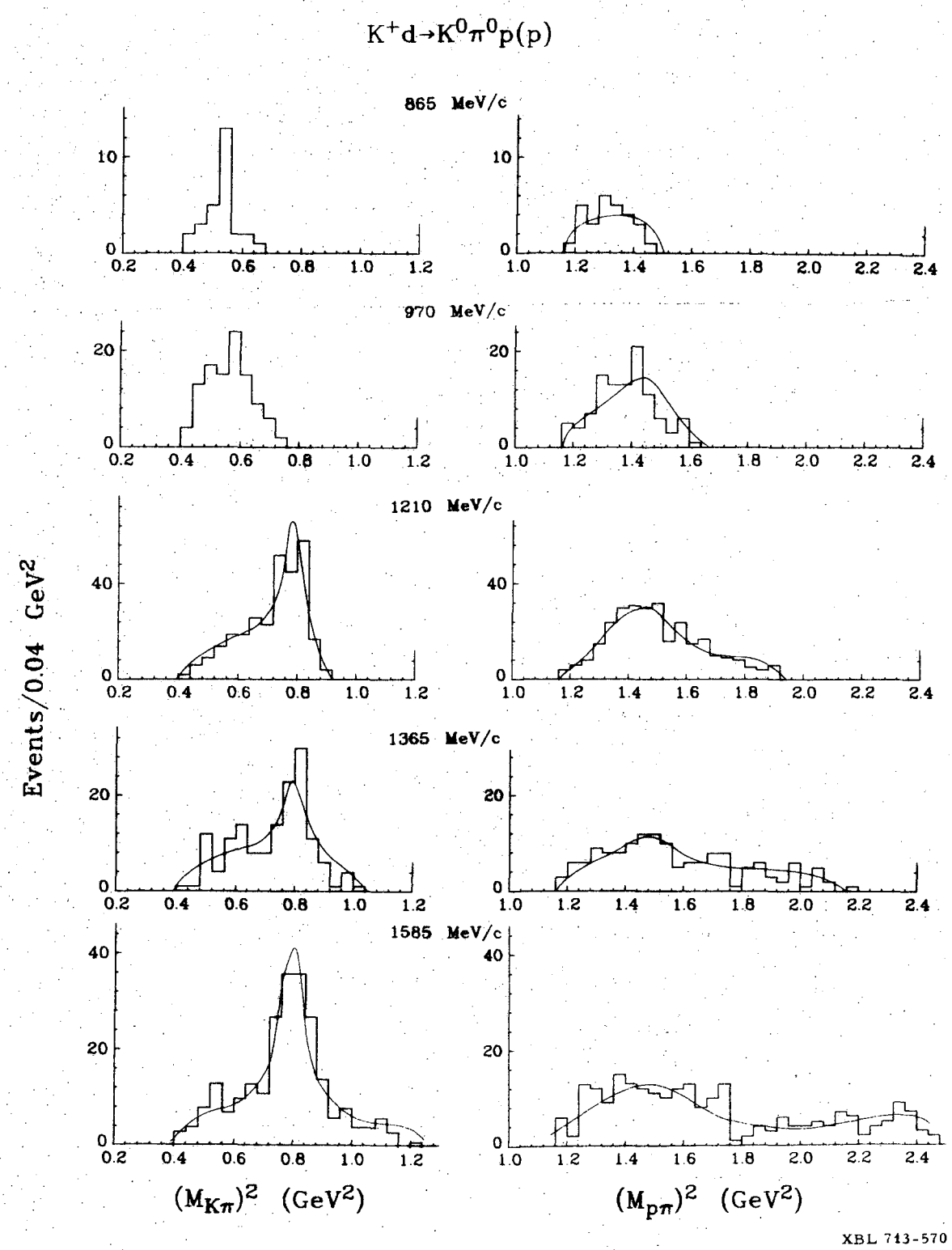

XBL 713-570

Fig. 7d

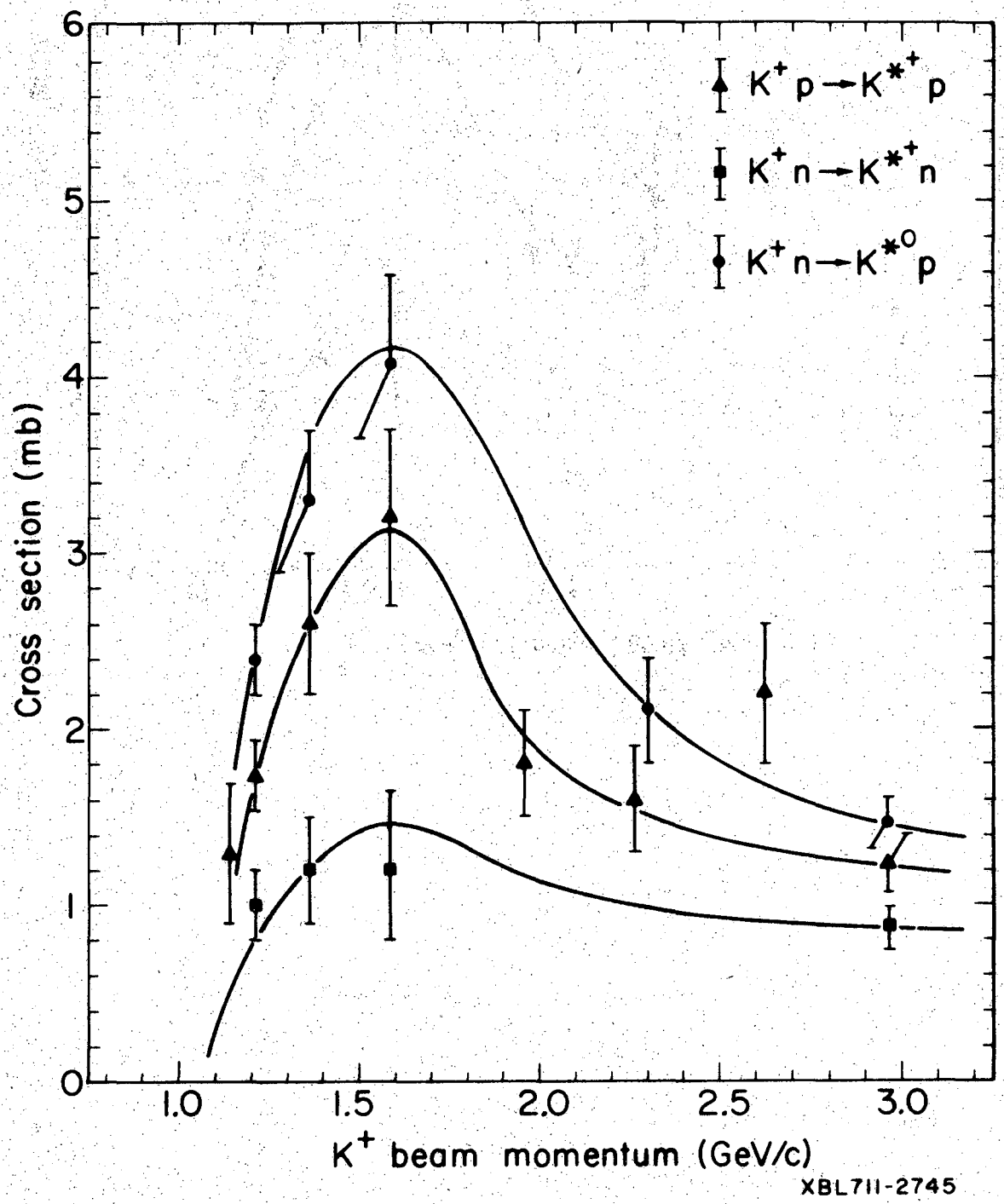
$K^+p \rightarrow K^{*+}p$
$K^+n \rightarrow K^{*+}n$
$K^+n \rightarrow K^{*0}p$
Cross section (mb)
0
1
2
3
4
5
6
1.0
1.5
2.0
2.5
3.0
K^+ beam momentum (GeV/c)
XBL711-2745

Fig. 8

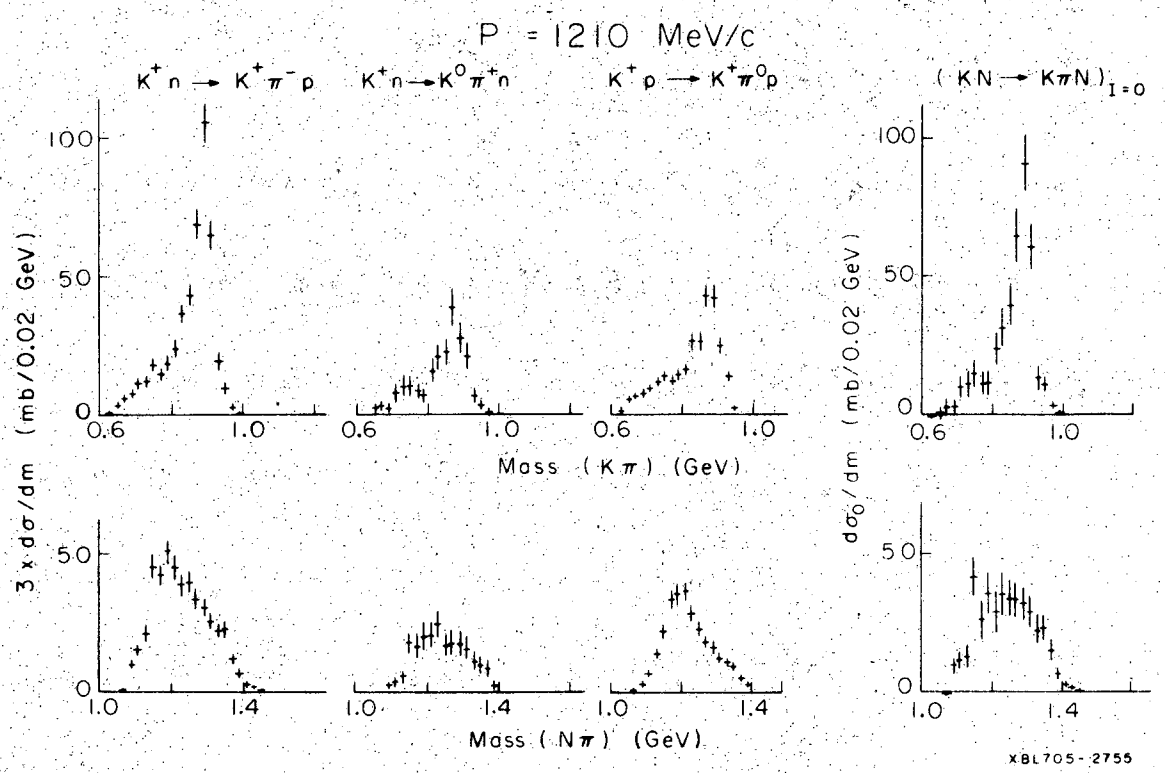
P = 1210 MeV/c
K+n → K+π−p
K+n → K0π+n
K+p → K+π0p
(KN → Kπ N)I=0
(mb/0.02 GeV)
Mass (Kπ) (GeV)
3 x dσ/dm
dσ0/dm
Mass (Nπ) (GeV)
XBL705-2755

Fig. 9

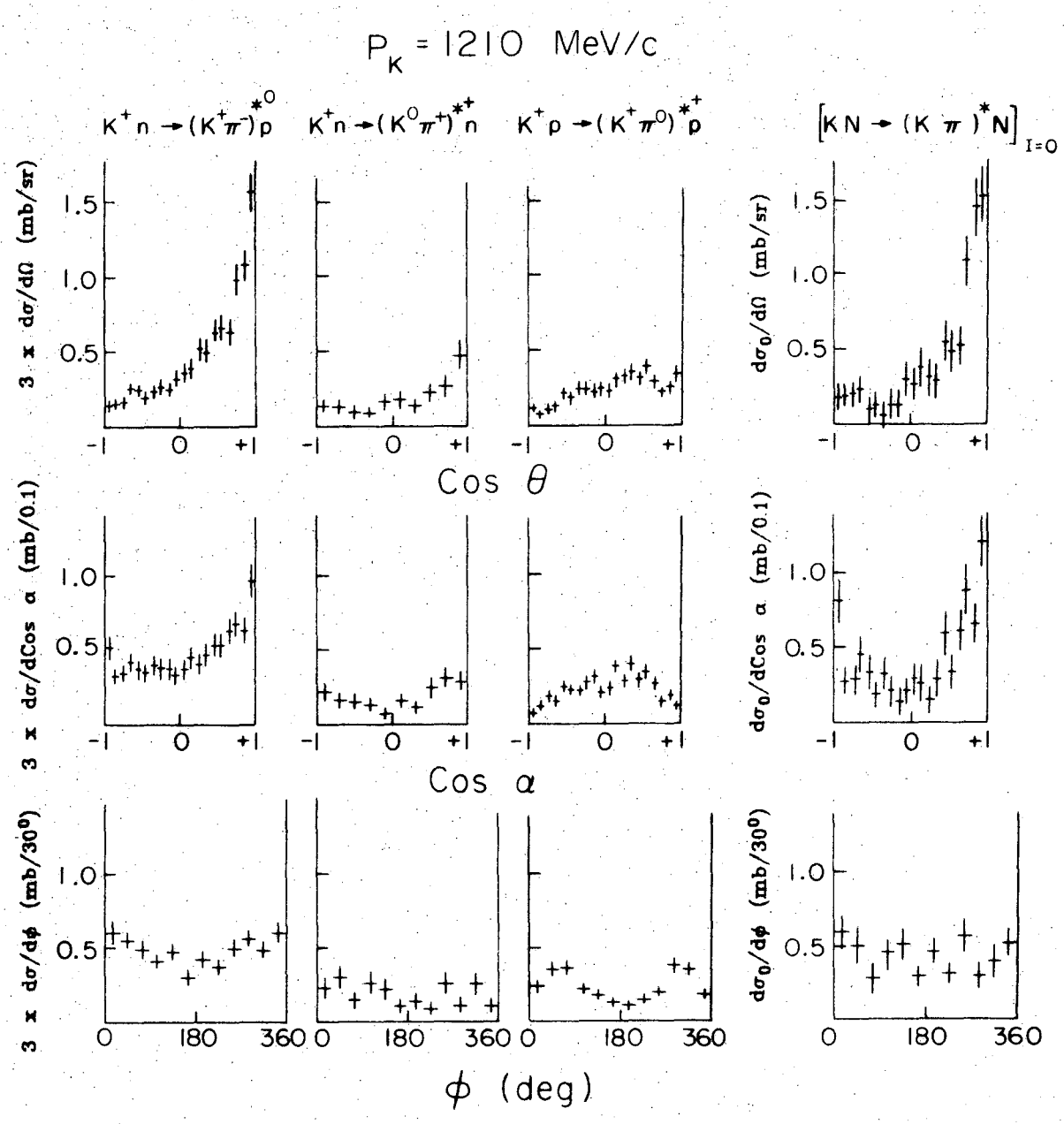

XBL705-2754

Fig. 10

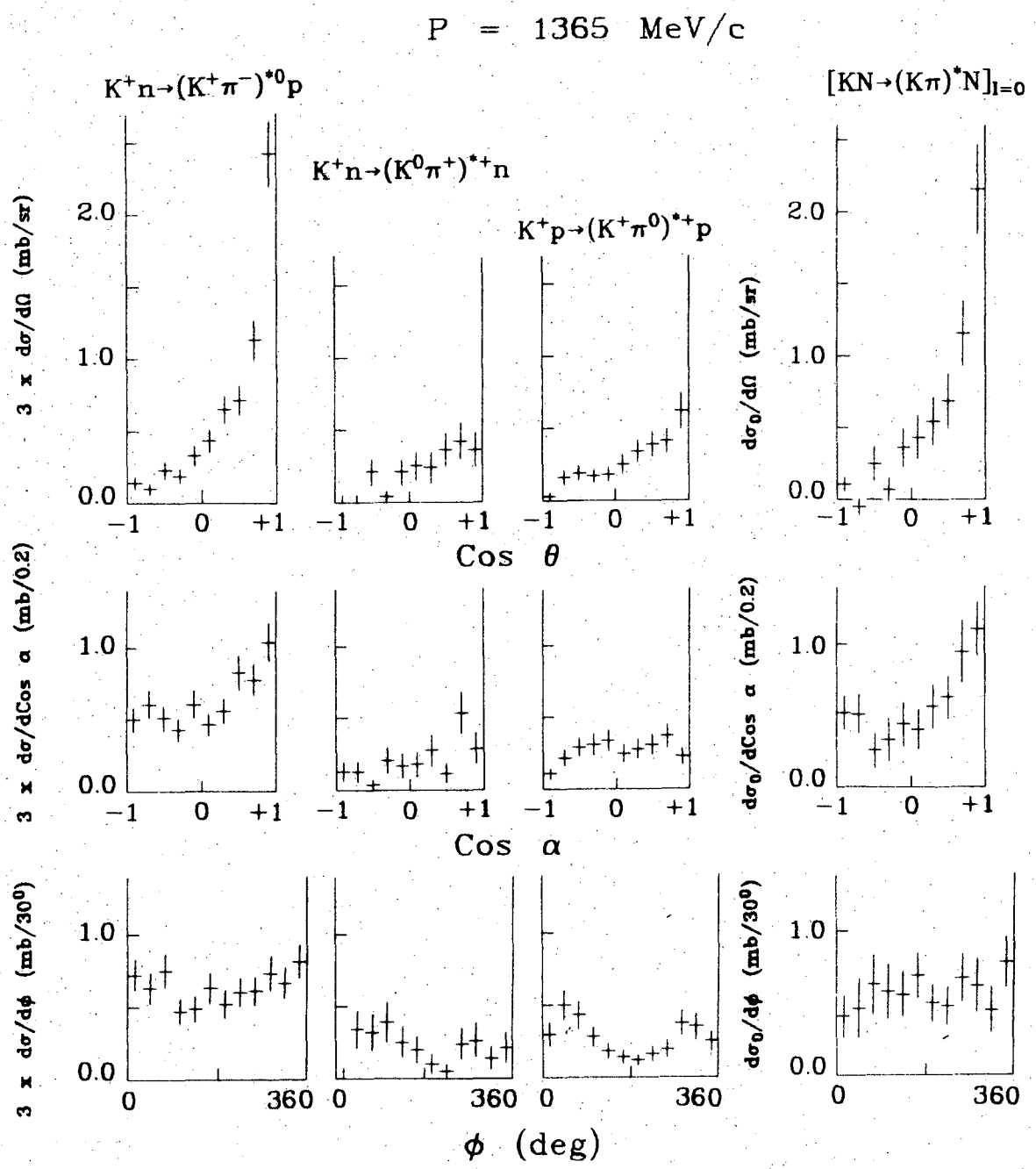
P = 1365 MeV/c
K+n→(K+π−)*0p
K+n→(K0π+)*+n
K+p→(K+π0)*+p
[KN→(Kπ)*N]I=0
3 x dσ/dΩ (mb/sr)
dσ0/dΩ (mb/sr)
Cos θ
3 x dσ/dCos α (mb/0.2)
dσ0/dCos α (mb/0.2)
Cos α
3 x dσ/dφ (mb/30°)
dσ0/dφ (mb/30°)
φ (deg)
XBL 7010-6683

Fig. 11

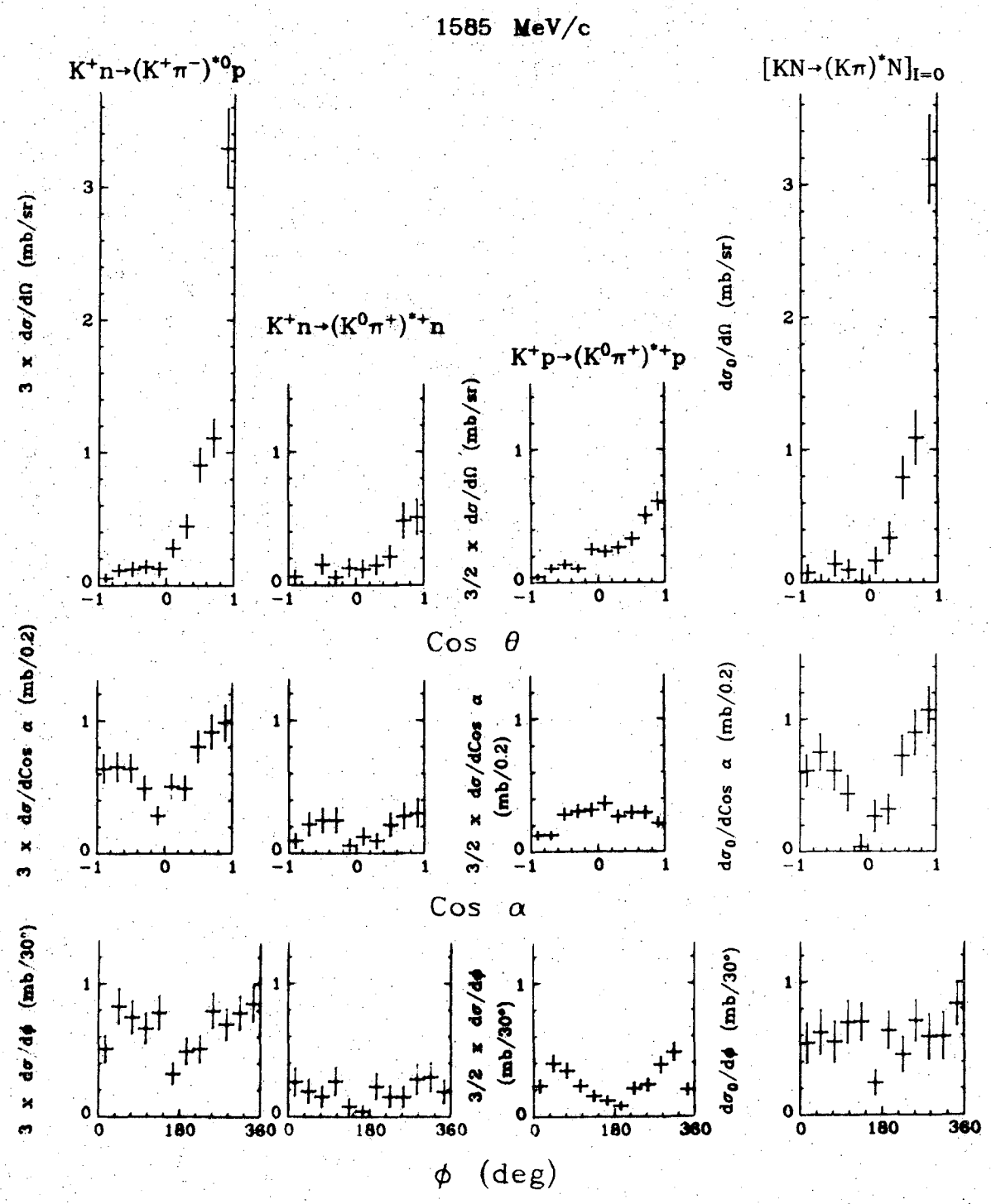

XBL 713-569

Fig. 12

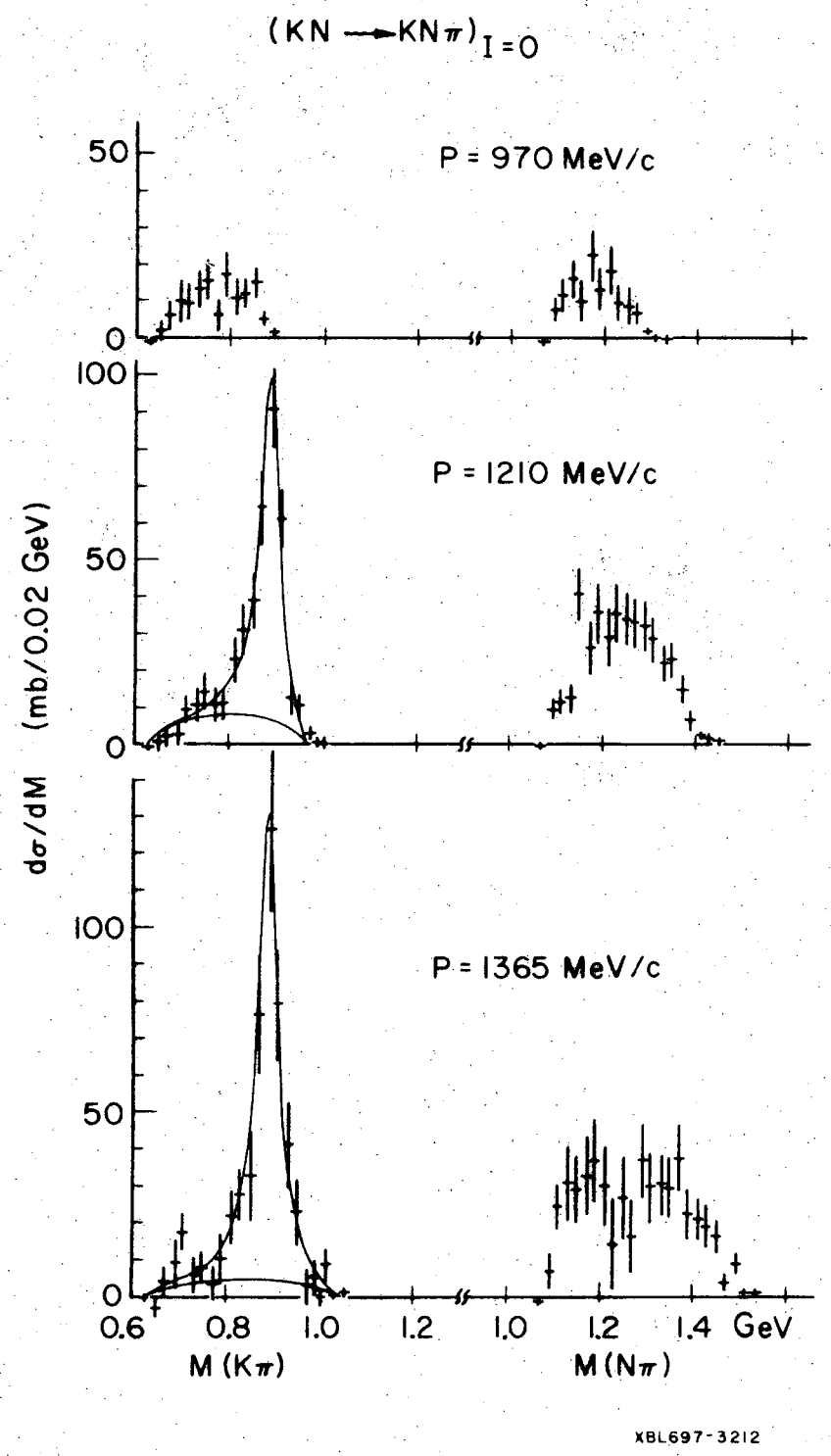
(KN → KNπ)I=0
P = 970 MeV/c
P = 1210 MeV/c
P = 1365 MeV/c
dσ/dM (mb/0.02 GeV)
50
0
100
50
0
100
50
0
0.6
0.8
1.0
1.2
1.0
1.2
1.4
GeV
M (Kπ)
M (Nπ)
XBL697-3212

Fig. 13

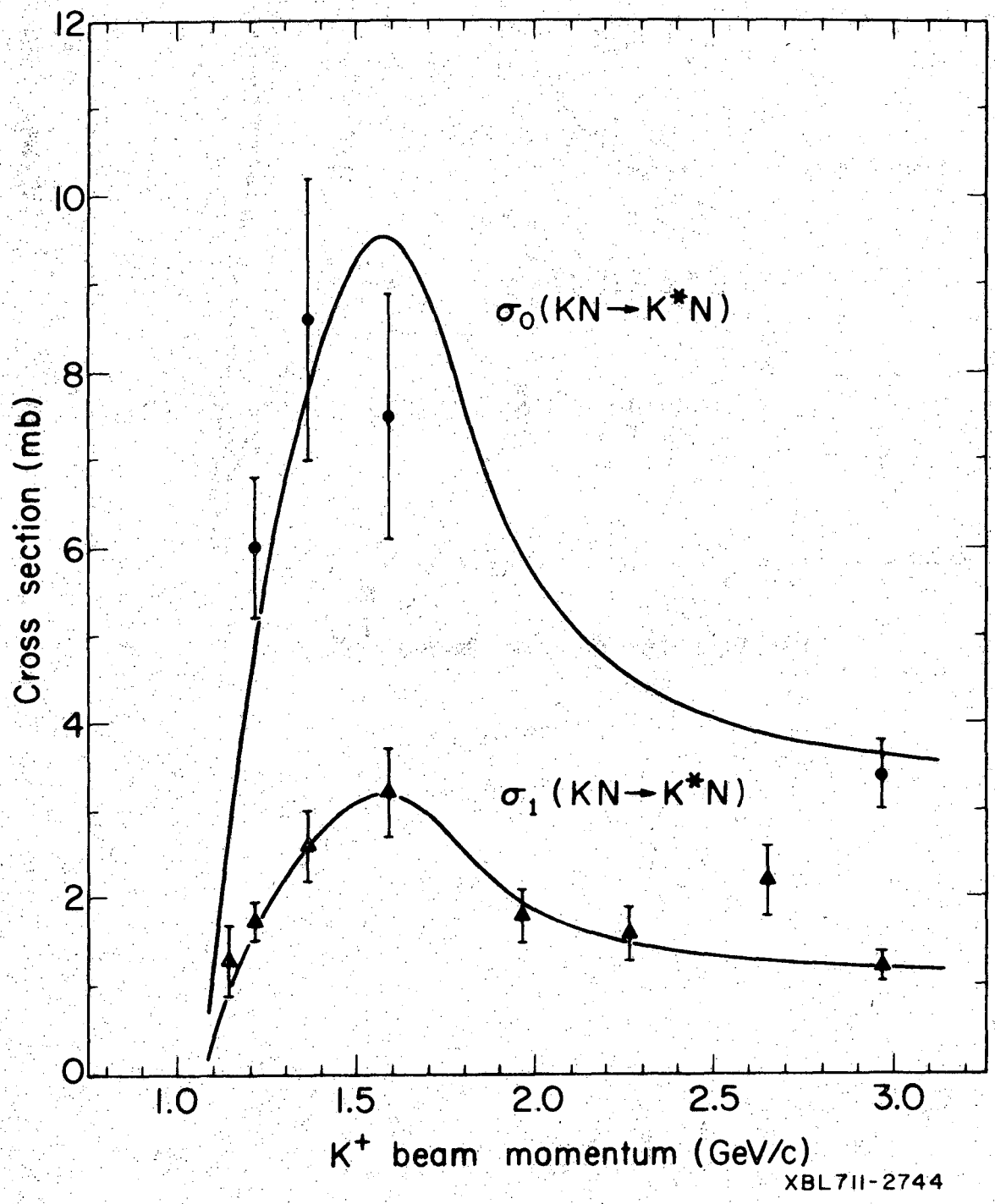
12
10
8
6
4
2
0
Cross section (mb)
$\sigma_0(KN \rightarrow K^*N)$
$\sigma_1(KN \rightarrow K^*N)$
1.0
1.5
2.0
2.5
3.0
K^+ beam momentum (GeV/c)
XBL711-2744

Fig. 14

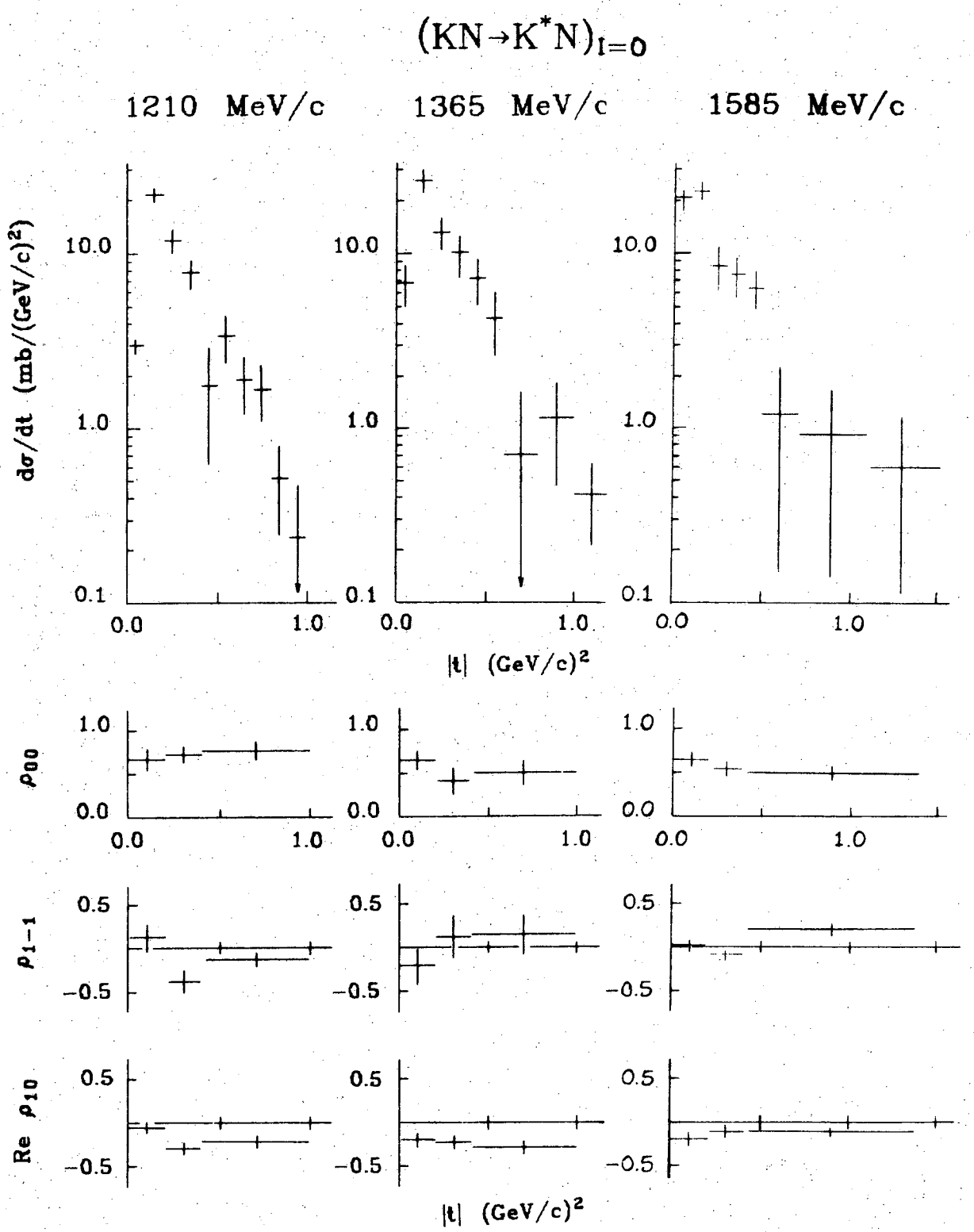

XBL 713-568

Fig. 15

LEGAL NOTICE

This report was prepared as an account of work sponsored by the United States Government. Neither the United States nor the United States Atomic Energy Commission, nor any of their employees, nor any of their contractors, subcontractors, or their employees, makes any warranty, express or implied, or assumes any legal liability or responsibility for the accuracy, completeness or usefulness of any information, apparatus, product or process disclosed, or represents that its use would not infringe privately owned rights.

TECHNICAL INFORMATION DIVISION
LAWRENCE RADIATION LABORATORY
UNIVERSITY OF CALIFORNIA
BERKELEY, CALIFORNIA 94720